

ABSTRACT

Title of dissertation: Terrace Width Distribution and First Passage Probabilities for Interacting Steps

Hailu Gebremariam Bantu
Doctor of Philosophy, 2005

Dissertation directed by: Professor Theodore L. Einstein
Department of Physics

Stochastic behavior of steps and inter-step distance is studied using Monte Carlo simulation. Terrace-step-kink model is used to represent vicinal surfaces. These vicinal surfaces consist of steps and the space between the steps called terraces.

In the first part, the distribution of the width of the terraces and its relation with the strength of step-step interaction is studied. Step positions on vicinal surfaces can be mapped into the world line of fermionic particles in one dimension. The distribution of the inter-particle distance in one dimension is in turn related to the distribution of energy levels one obtains from Random Matrix theory. The energy level distribution in Random Matrix theory is nicely approximated by Wigner distribution for three symmetries described by three parameters. These parameters correspond to the step-step interaction strength in vicinal surfaces. However, when we consider vicinal surfaces the three values of step-step interaction strength are not special. Therefore, they are generalized to include all interaction strengths and

it is called the generalized Wigner distribution. The Monte Carlo simulation results show that the generalized Wigner distribution is a very accurate description for the terrace width distribution.

Analytical and simulation results of study of the evolution of the variance of the terrace width distribution for different physically interesting and experimentally testable situations are also presented. The analytical result is based on Fokker-Planck formalism obtained from the mapping of the vicinal surfaces into one-dimensional spinless fermionic particles.

In the second part, we present the study of the effect of step-step interaction on several scaling laws one obtains from the Langevin formalism of step fluctuations. Based on the limiting processes responsible for fluctuations of isolated step, the mechanisms are divided into three universality classes: attachment-detachment, step-edge diffusion and terrace diffusion. Using Monte Carlo simulation of an attachment-detachment type process, we show that the scaling laws for width of fluctuation, correlation time and survival probabilities are affected by interaction of steps. In contradiction to what one expects from the analytical results obtained using the Gruber-Mullins picture, We also show that the correlation time increases with interaction strength.

Terrace Width Distribution and First Passage Probabilities for
Interacting Steps

by

Hailu Gebremariam Bantu

Dissertation submitted to the Faculty of the Graduate School of the
University of Maryland, College Park in partial fulfillment
of the requirements for the degree of
Doctor of Philosophy
2005

Advisory Committee:

Professor Theodore L. Einstein, Chair/Advisor
Professor Ellen D. Williams
Professor John D. Weeks
Professor Victor M. Yakovenko
Professor Jian-Guo Liu

© Copyright by
Hailu Gebremariam Bantu
2005

This dissertation is dedicated to my family.

ACKNOWLEDGMENTS

I owe my gratitude to all the people who have made this thesis possible and because of whom my graduate experience has been memorable.

First and foremost I'd like to thank my advisor, Professor Theodore L. Einstein for giving me an invaluable opportunity to work on challenging and interesting projects. He has always made himself available for help and advice and there has never been an occasion when I've knocked on his door and he hasn't given me time.

I would also like to thank Professor Chandan Dasgupta for giving me his invaluable advise on the second part of this thesis. I owe him my sincere thanks for everything I learned about autocorrelation, persistence and survival probability from our communication, in person and via email. Thanks are due to Professor Ellen D. Williams, Professor John D. Weeks, Professor Victor M. Yakovenko and Professor Jian-Guo Liu for agreeing to serve on my dissertation committee and for sparing their invaluable time reviewing the manuscript. I am also indebted to Professor Michael Coplan for his help in administrative and academic issues that I have come across throughout my graduate studies in the chemical physics program.

My colleagues at the surface Physics group have enriched my graduate life in many ways and deserve a special mention. My discussions with graduate students Timothy Stasevcih (Tim) and Masashi Degawa (Tosh) have great contribution to my understanding of surface properties. Besides Physics, I benefited from our discus-

sions about life and social problems in the whole world. Former graduate students Magdalena (magda) Constantin and Daniel (Dan) Dougherty have helped me a lot in understanding persistence properties. I have gained a lot in programming and using the UNIX effectively, from my interaction with Dr. Ferenc Szalma and Dr. William (Bill) Cullen.

I would also like to acknowledge the financial support I received from MRSEC. My sincere thanks are due to MRSEC staff for their help and support in many ways because without their help I don't think I would meet many deadlines.

I owe my deepest thanks to my family - my mother, my father, my brother and my sister who have always stood by me and morally support me from across the ocean.

It is impossible to remember all, and I apologize to those I've inadvertently left out.

Lastly, thank you all and thank God!

TABLE OF CONTENTS

List of Tables	vii
List of Figures	viii
1 Terrace Width Distribution	1
1.1 Overview	1
1.2 Theoretical works	5
1.2.1 Mean field approach	5
1.2.2 Random Matrix ideas [18]	9
1.2.3 Spinless fermions in one dimensions	11
1.2.4 Terrace width distribution	14
2 Monte Carlo Simulation - Terrace Width Distribution	16
3 Fokker-Planck Derivation of Evolution of Terrace-width Distribution	24
3.1 Motivation	24
3.2 The Fokker-Planck Derivation	25
4 Stochastic description of fluctuating steps	35
4.1 Motivation	35
4.2 Langevin Formalism	35
4.3 First Passage Probabilities	45
4.4 Step-Step Interaction included	49

5	Monte Carlo Simulation - Step Fluctuation	52
5.1	Motivation	52
5.2	Isolated Step	53
5.2.1	Width	54
5.2.2	Correlations	55
5.2.3	Persistence and survival probability	59
5.3	Interacting Steps	63
5.3.1	Width	64
5.3.2	Time correlation and persistence	64
5.3.3	Autocorrelation and survival probability	67
6	Conclusion	76
	Bibliography	82

LIST OF TABLES

5.1	The measured correlation time, survival time and their ratio as the interaction strength is increased: The upper table for A/l^2 potential for $A = 0.0$ to $A = 4.0$ and the lower one for confining harmonic potential λ varying from $\lambda = 0.000$ to $\lambda = 0.015$	74
-----	--	----

LIST OF FIGURES

1.1	Steps and kinks on a typical fcc surface with high Miller indices (from ref [8])	2
1.2	A vicinal surface in the continuum step model	3
1.3	a) The step in between two fixed walls b) The terrace width distribution in terms of $s=x/L$	6
1.4	The variance as a function of the dimensionless interaction strength in the Gruber-Mullins approximations for the case nearest neighbors(dashed line), and all step (solid line) interactions. The dotted line shows the Grenoble group's result.	8
2.1	Top view of a typical surface discrete both in the x- and y-direction. .	16
2.2	Typical plot of variance as a function of the Monte Carlo steps per site (MCS)	18
2.3	A linear fit with a log-log plot.	19
2.4	The measured variance as a function of the number of steps N and step length L_y	21

2.5 Comparison of the measured value of the variances (MC) with the expected values from the generalized Wigner distribution(GW), Gruber-Mullins with nearest neighbor interaction(GMN), Gruber Mullins with all steps interaction(GMA) and the Grenoble’s group modification(GN). (a) σ^2 vs \tilde{A} ; (b) $\varrho\sigma^2$ vs \tilde{A} 22

3.1 The graph of first moment predicted using the Fokker-Planck analytical prediction for an initially perfectly-cleaved crystal with $\tilde{A} = 0$, $\varrho = 2$ 30

3.2 Comparison of the variance predicted using the Fokker-Plank analytical prediction(dashed lines) and the variance computed using conventional Metropolis Monte-Carlo for a terrace-step-kink model(solid lines). The upper curves are for “free fermions” ($\tilde{A} = 0$, $\varrho = 2$). Both upper curves approach the equilibrium variance $\sigma_\infty^2 = 0.18$ [4]. The lower pair of curves show the predicted(dashed) and computed (solid) variances for $\tilde{A} \approx 2.762$, $\varrho \approx 4.47$, with a different scaling factor between \tilde{t} and MC time. Both lower curves approach $\sigma_\infty^2 = 0.095$. The left and right inset panels show the initial and a typical late-time configuration of the steps in the Monte Carlo simulation, respectively. 32

4.1 Schematic diagram of the two common limiting processes: Attachment-Detachment (AD) and Step-Edge-Diffusion limiting processes. 36

5.1	Typical TSK representation of an isolated step.	53
5.2	Typical plot of width as a function Monte Carlo time for two step lengths: the lower: $L_y = 100$, upper: $L_y = 200$	55
5.3	The log-log plot of saturation value of the width W_{sat} as a function of step length L_y . The points are found from the simulation. The straight line fit gives a slope of 0.51.	56
5.4	The log-log plot of time correlation function (G) as a function of time in MCS with a straight line fit of slope = 0.499.	57
5.5	The semi-log plot of autocorrelation function ($C(t)$) as a function of time in MCS for a step length of $L_y = 100$ with the fitting line for the long time part.	58
5.6	The log-log plot of correlation time (τ_c) as a function of L_y . The points are found from the simulation. The line is the fit to the points giving slope = 1.99.	59
5.7	The log-log plot of persistence as a function of time in MCS with a straight line fit of the long time part. The slope measured is $\theta = 0.76$	60
5.8	The semi-log plot of survival as a function of time in MCS with the linear fit to the long time part.	61

5.9 (a)The semi-log plot of autocorrelation as a function of time for step length $L_y = 100$ with two different sampling time $\delta t = 4$ and 5. (b) Semi-log plot of the survival probability versus time for step length $L_y = 50$ with different sampling times $\delta t = 4$ and 5. 62

5.10 The semi-log plot of survival probabilities for three different lengths $L_y = 50, 100, 150$ with three different sampling times $\delta t = 1, 4, 9$, respectively, keeping the ratio $\delta t/L_y^z$ constant. (a) showing poor collapse for $z= 2.0$, (b) the best collapse for $z = 1.92$ 63

5.11 The plot of the width as a function of time for a system of 4 steps, length $L_y = 200$, average inter-step distance $L = 10$ and three different interaction strengths. The upper curve is for interaction strength $A = 0$, the middle curve is for $A = 2$, the lowest curve is for $A = 10$. . . 65

5.12 The log-log plot of the saturation width versus length of step for 4 interacting steps. (a) Interaction strength $A = 0$ and the fitting line has a slope 0.43, (b) $A=2.0$ and the straight line fit gives a slope of $\alpha = 0.31$ 65

5.13 A typical log-log plot of time correlation as a function of time in MCS for 4 interacting steps with interaction strength:(a) $A = 0$, the slope of the fit line is 0.500, (b) $A = 2$, the measured slope by fitting is 0.488. 67

5.14	A typical log-log plot of persistence as a function of time in MCS for 4 interacting steps with interaction strength: (a) $A = 0$ and the slope of the fit is 0.77 and (b) $A = 2$ where it is fitted to a line of slope 0.82	67
5.15	Semilog plot of autocorrelation as a function of time in MCS for 4 interacting steps with interaction strength $A = 0, 2,$ and $8.$	68
5.16	Semilog plot of autocorrelation as a function of time obtained by integrating Eq.(4.36) from ref.[48] assuming confining harmonic potential with interaction strength $\lambda = 0, 0.002, 0.005, 0.010,$ and $0.015.$	69
5.17	Semilog plot of autocorrelation as a function of time obtained from Monte Carlo Simulation using confining harmonic potential with interaction strength $\lambda = 0, 0.002, 0.005, 0.010,$ and $0.015.$	70
5.18	Semilog plot of autocorrelation as a function of time obtained from Monte Carlo simulation using moving confining harmonic potential with interaction strength $\lambda = 0, 0.1, 0.5,$ and $0.8.$	71
5.19	Semilog plot of survival probability as a function of time in MCS for 4 interacting steps of length $L_y = 100$ with interaction strength $A = 0, 0.5, 1.0, 1.5, 2.0.$	73

- 5.20 The semilog plot of survival probability as a function of t/Ly^z for systems of different three different lengths, $L_y = 100, 150, 200$, but the same $\delta t/Ly^z$. The left and right panels are for $A = 0.000$ and $A = 0.362$, respectively. 75
- 5.21 The semilog plot of survival probability as a function of t/τ_c for systems of different three different lengths but the same $\delta t/\tau_c$. The left panel is for $L_y = 100, 150, 200$ with $A=0.000$ and the right panel is for $L_y=100, 151, 200$ with $A=0.362$ 75

Chapter 1

Terrace Width Distribution

1.1 Overview

One of the fundamental questions of surface science asks how the morphology of a surface is related to surface energetics. In an effort to answer this question several works have been done using equilibrium thermodynamics to determine the orientational dependence of surface free energy [1]. This orientational variation depends on the energies of steps and their interactions. During the last decade, step dynamics and step-step interactions have been extensively studied for well-ordered vicinal surfaces [2, 3, 4, 5, 6, 7]. These surfaces consist of nearly parallel steps with an average terrace width that depends on the angle between the vicinal surface and the nearest energetically preferred (low-index) surface. A typical vicinal surface is shown in Fig. 1.1.

The practical reasons to understand this aspect of a surface stems from the idea to develop novel materials whose properties lie in the length scale from nanometers to microns. In this length scale properties of a material are strongly influenced by finite-size effects occurring at the atomic scale. A complete description of such influences can not be found from continuum mechanics or from an extrapolation of individual atomic behavior. In order to include the atomic behaviors while having the computational simplification of continuum mechanics, a continuum step model

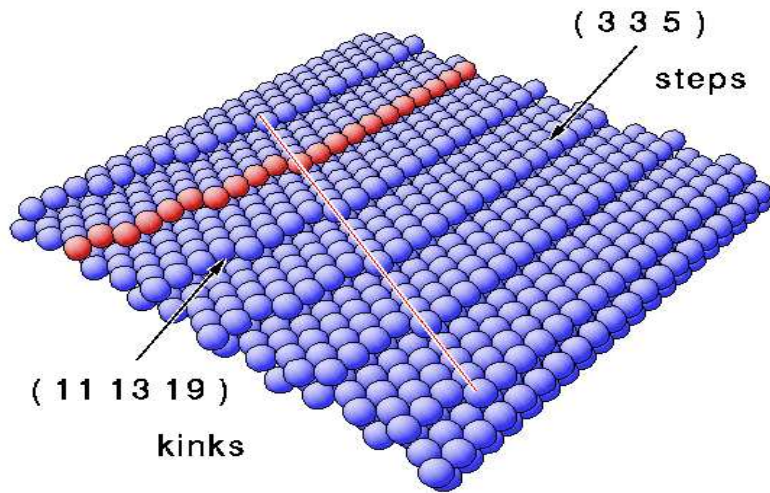


Figure 1.1: Steps and kinks on a typical fcc surface with high Miller indices (from ref [8])

is found to be extremely powerful. As shown in the figure 1.2, a vicinal surface consists of steps which are represented as continuous functions along the step-edge and as discrete functions perpendicular to the step-edge.

In the continuum step model, evolution of surface morphology is described in terms of the motion of steps, which is implicitly connected to atomic motion via the attachment and detachment of atoms at the step-edge. The addition and removal of atoms on and from the step-edge correspond to formation or motion of kinks.

We will be focusing on the steps moving under the influence of temperature only, which means the kinks under consideration are assumed to be formed due to the temperature; thus, they are called thermal kinks. The steps are caused by miscuts and are therefore forced or geometric. For a vicinal surface of certain size,

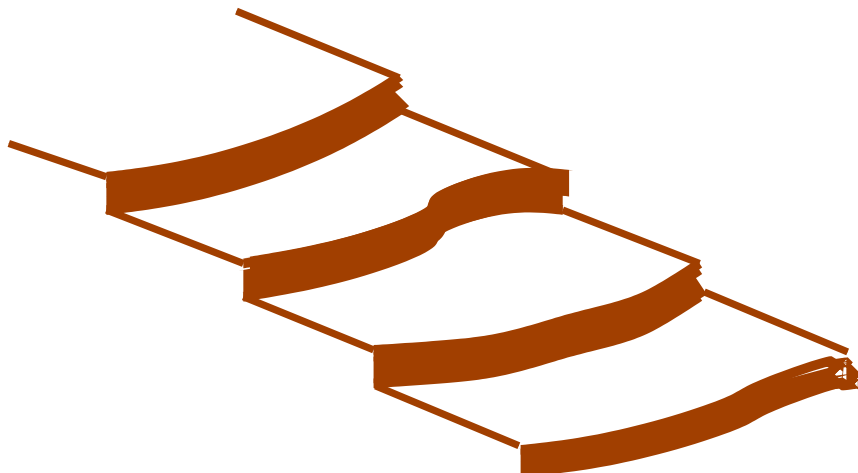


Figure 1.2: A vicinal surface in the continuum step model

the number of steps is fixed by the misorientation angle. These steps are separated by a terrace which has a high-symmetry direction. The measurement of the width distributions of these terraces can be used to study the interaction between the steps. These interactions, in addition to step stiffness, are very important in determining the morphology of surfaces.

Developments in surface imaging techniques, such as scanning tunneling microscopy (STM)[9], low energy electron microscopy (LEEM), reflection electron microscopy (REM), have made it possible to measure directly the terrace width distributions (TWD). These measurements contain information about both the thermal excitations of the step edge and the nature of the step-step interactions. The form of these interactions is difficult to prove solely from the terrace width distributions. However, physical considerations can give us some information. If we bring steps close to one another, since they do not cross, the amount of wandering of these steps will decrease, as will the configurational entropy, leading to an effective entropic re-

pulsion that varies as the inverse step-separations (l) squared with a proportionality constant A_{entropic} , $U_{\text{entropic}} = A_{\text{entropic}}/l^2$. This entropic repulsion is manifested in the distribution of the steps. A step which is midway between its neighbors has more configurational entropy than one which is near its neighbors, and thus the terrace-width distribution will peak near the average step-separation [10, 11, 12]. The distribution for the case where all the steps are wandering simultaneously can be solved exactly[10]. This distribution, scaled by the average terrace width, has a universal form in the sense that it will be the same for any system regardless of the average terrace-width. Deviations from this universal form can be used to deduce the presence of energetic interactions between steps. If there are attractive interactions too weak to overcome the entropic repulsion, the distribution will be broader, and the peak moves to a smaller value than the average terrace-width. If there are repulsive interactions, the distribution becomes narrower.

Statistical analysis of the TWDs provides a method to obtain quantitative values for the parameters characterizing the strength of step-step interaction. The most important kinds of energetic interactions are elastic and electronic in nature. Interestingly, both elastic and dipole-dipole interactions behave as A/l^2 as a function of l and another proportionality constant A [14]. Elastic interactions are always repulsive, whereas electric dipole-dipole interactions may have either sign [7]. Although the entropic and the energetic interactions have the same dependence on the step-separation, they do not add up simply[14].

A detailed study of the terrace width distributions (TWD) reveals that the proportionality constant (A) is related to the variance of the TWD. Theoretical

studies have been done to find this relation assuming different approximations for the step-step interactions. In this chapter these analytical results are reviewed.

1.2 Theoretical works

1.2.1 Mean field approach

In this approach a step is assumed to be wandering between two steps fixed at $x=0$ and $x=2L$. It was used first by Gruber and Mullins [13] and is sometimes referred to as the Gruber-Mullins approach.

Since step overhangs are physically forbidden and there are no islands, the step configurations in 2D space map into the world lines of spinless fermions in one dimension [10]. In this mean field approach, if we assume the steps only interact entropically, a step can be considered as a free particle in a box of size twice the mean-terrace-width. For such a particle in a box, writing a Schrödinger equation in terms of $s = x/L$ one finds that the ground state wave function and the probability density (fig(1.3)) is

$$P(s) = \sin^2\left(\frac{\pi s}{2}\right) \quad (1.1)$$

We know that the steps interact with each other. We may therefore add interaction into this system. Let us say the interaction potential due to each neighboring step is known. The potential felt by the wandering step is then

$$V(x) = U(x) + U(2L - x) \quad (1.2)$$

Assuming that the step fluctuates around $x = L$ and this fluctuation is small

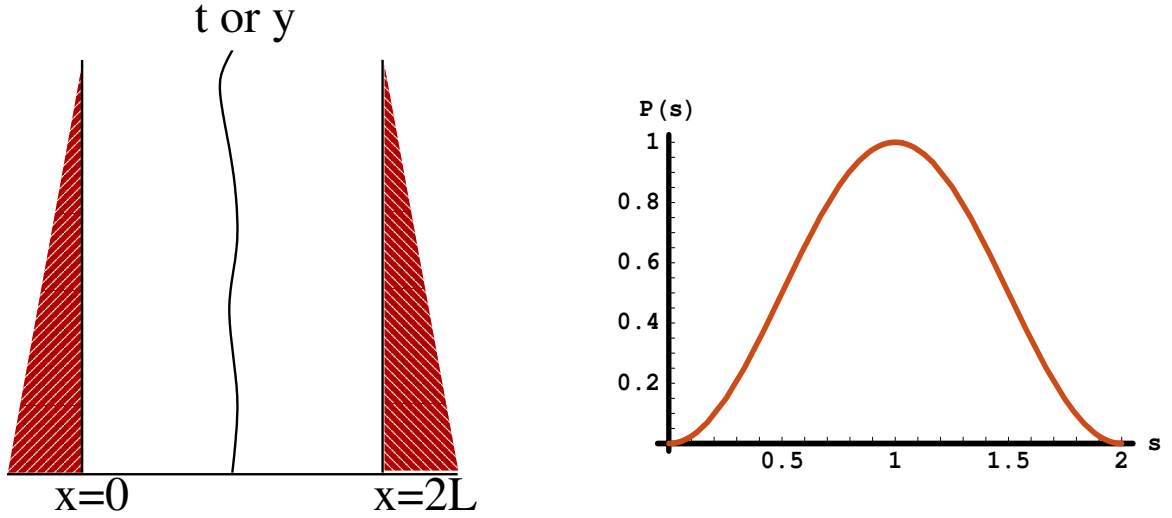


Figure 1.3: a) The step in between two fixed walls b) The terrace width distribution in terms of $s=x/L$

compared to the width, we can expand the potential of the step about $x = L$ and keep terms up to second order only:

$$V(x) = 2U(L) + U''(L)(x - L)^2 \quad (1.3)$$

Again, looking at this step as a world line of a particle under such a potential, which happens to be a simple harmonic, and using the ground state wave function for a simple harmonic oscillator, the probability density is given by

$$P(x) = \frac{1}{W\sqrt{2\pi}} \exp\left(-\frac{(x - L)^2}{2W^2}\right) \quad (1.4)$$

where $W^2 \propto U''(L)^{-1/2}$.

This suggests that the terrace width distribution (TWD) has a Gaussian form. By convention it can be written in terms of the dimensionless parameter $s = x/L$.

This gives us a TWD that is not just normalized but has unit mean. The form of the Gaussian approximation is then

$$P(s) = \frac{1}{\sqrt{2\pi}\sigma} \exp\left[-\frac{(s-1)^2}{2\sigma^2}\right] \quad (1.5)$$

The interaction between steps can be due to elastic or dipole-dipole interactions. For these kind of interactions, the potential has the form [14]

$$U(x) = \frac{A}{x^2} \quad (1.6)$$

which means

$$\sigma^2 = \hat{K} A^{-1/2} \quad (1.7)$$

where \hat{K} is some constant.

This result has a great significance in determining the interaction strength A by measuring the terrace width distribution. It means if one can get the variance of the terrace width distribution, one can get the interaction strength. In fact a dimensionless interaction strength \tilde{A} is defined as

$$\tilde{A} = \frac{A\tilde{\beta}}{(k_B T)^2} \quad (1.8)$$

where $\tilde{\beta}$ is the stiffness of the step. Thus the variance can be written in a simple form

$$\sigma^2 = K_{GM} \tilde{A}^{-1/2} \quad (1.9)$$

where $K_{GM} = 1/\sqrt{48}$. The subscript GM is to show it is in the Gruber-Mullins approximation.

This method has three limitations: first, the interactions considered are only nearest neighbor; second, it does not take the fluctuations of the neighboring steps into consideration; and third, it has been approximated by expanding the potential to second order only.

The first limitation can be lifted by considering interaction among all steps. The form of the relationship between the variance and the interaction strength remains the same with a different proportionality constant $K_{GMall} = \sqrt{15/8\pi^4}$ [17].

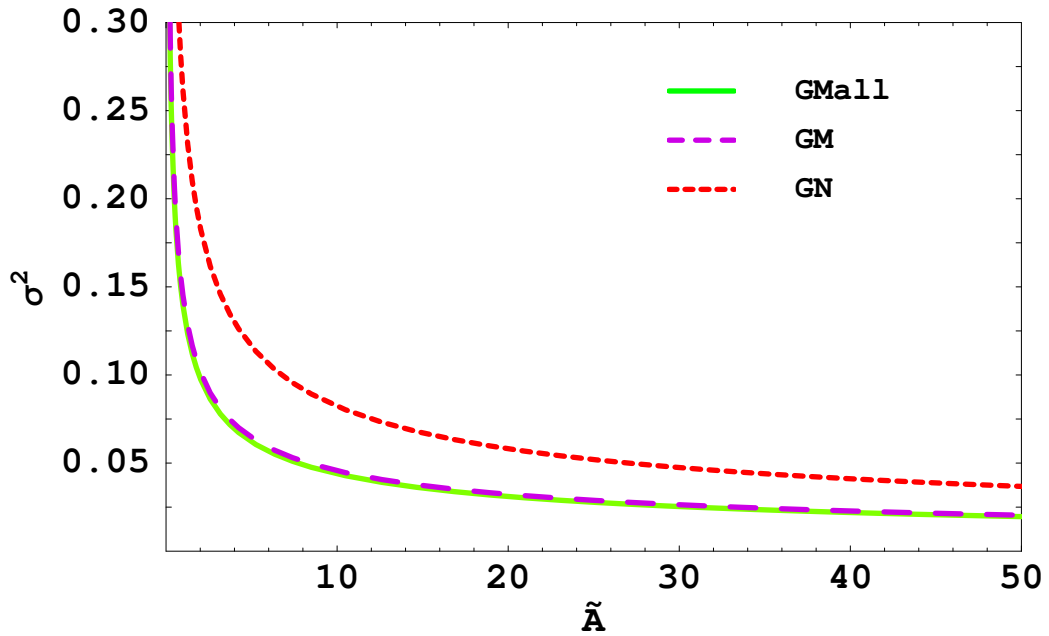


Figure 1.4: The variance as a function of the dimensionless interaction strength in the Gruber-Mullins approximations for the case nearest neighbors(dashed line), and all step (solid line) interactions. The dotted line shows the Grenoble group's result.

The second point was raised and discussed by the Grenoble group [24]. They pointed out that the Gruber-Mullins's approach underestimates the variance for a given \tilde{A} . If both steps bounding the fluctuating step are allowed to fluctuate independently, then the variance of the TWD should be the sum of the variances of the fluctuations of the two steps bounding it. As a result of this, the proportionality constant becomes $K_{GN} = 1/\sqrt{14.80}$.

The graph above shows the different approximate relations of the variance with the dimensionless interaction strength \tilde{A} . All of these distributions are Gaussian distributions and they have been used to analyze several experimental works discussed in the standard review papers[2, 3].

1.2.2 Random Matrix ideas [18]

In the theory of random matrices one is concerned with ensembles of matrices whose elements are random variables with given probability distributions. The question is then what can one say about the probabilities of a few of its eigenvalues and the spacings between eigenvalues. This will be connected to the terrace width distribution of a vicinal surface through the probability distribution of fermions in one dimension with a certain type of interaction.

In mathematical models, systems are characterized by their Hamiltonians, which in turn are represented by Hermitian matrices. We will consider matrices whose elements may be supposed to be random variables and allowed the maximum statistical independence permitted under symmetry requirements. The three ensembles of Hamiltonians we consider are orthogonal, unitary and symplectic in

nature.

In each of these cases the joint probability density function $P(H)$ is invariant under a nonsingular similarity transformations

$$H \longrightarrow H' = AHA^{-1}. \quad (1.10)$$

Such an invariant can be expressed in terms of the traces of the first N powers of H and the form of $P(H)$ is restricted to [18]

$$P(H) = \exp(-a\text{Tr}H^2 + b\text{Tr}H + c), \quad (1.11)$$

where a is real and positive, and b and c are real. If $P(H)$ depends only on the traces of powers of H , then the joint probability density of the eigenvalues will contain a factor coming from the Jacobian of the elements of H with respect to its eigenvalues. For random Hermitian matrices H , the joint probability density $P_{N\varrho}$ of its real eigenvalues x_1, x_2, \dots, x_N is

$$P_{N\varrho} = C \prod_{1 \leq j < k \leq N} |x_j - x_k|^\varrho \exp(-\frac{1}{2}\varrho \sum_{j=1}^N x_j^2/2), \quad (1.12)$$

where $\varrho = 1, 2$, or 4 , depending on whether the ensemble is Gaussian orthogonal, Gaussian unitary, or Gaussian symplectic. The proportionality constant can be chosen in such a way that $P_{N\varrho}$ is normalized to unity.

$$\int_{-\infty}^{\infty} \dots \int_{-\infty}^{\infty} P_{N\varrho}(x_1, \dots, x_N) dx_1 \dots dx_N = 1. \quad (1.13)$$

According to Selberg [18] the normalization constant is given by

$$C^{-1} = (2\pi)^{N/2} \varrho^{-N/2 - \varrho N(N-1)/4} [\Gamma(1 + \varrho/2)]^{-N} \prod_{j=1}^N \Gamma(1 + \varrho j/2). \quad (1.14)$$

The nearest-neighbor spacing distribution $P(s)$, which is the probability density for two neighboring levels to have spacing s , is the observable most commonly used to study the short-range fluctuations in the spectrum. The function $P(s)$ and its first moment are normalized to unity,

$$\int_0^\infty P(s) ds = 1 \quad \text{and} \quad \int_0^\infty s P(s) ds = 1. \quad (1.15)$$

The analytical calculation of $P(s)$ from the correlation functions is possible but highly non-trivial, involving infinite products [18]. A very good approximation is given by the Wigner surmise

$$P(s) = a_\varrho s^\varrho \exp(-b_\varrho s^2) \quad (1.16)$$

for all three symmetry classes with $\varrho = 1, 2, 4$. The constants are given by [20]

$$a_\varrho = 2 \frac{\Gamma^{\varrho+1}((\varrho+2)/2)}{\Gamma^{\varrho+2}((\varrho+1)/2)} \quad \text{and} \quad b_\varrho = \frac{\Gamma^2((\varrho+2)/2)}{\Gamma^2((\varrho+1)/2)}. \quad (1.17)$$

1.2.3 Spinless fermions in one dimensions

The problem of system of fermions in one dimension with $1/l^2$ repulsions was solved by Calogero [21] and Sutherland[22]. Both works are quite similar in their analysis but I will follow the Sutherland work because it is related more directly to what will be discussed here.

The basic idea is to find the ground state wave function of an N -particle system in one dimension whose Hamiltonian is given by

$$H = -\sum_{i=1}^N \frac{\partial^2}{\partial x_i^2} + \prod_{i<j} \frac{A}{(x_i - x_j)^2} + \omega^2 \sum_{i=1}^N x_i^2, \quad (1.18)$$

where the second and third term are the potential terms. The second term represents the repulsive interaction with strength A , and the third term is a confining potential keeping the particles from flying apart due to the repulsive interaction. This Hamiltonian will be exactly what we will have for our system when $\omega \rightarrow 0$, which is also the same as taking the limit $N \rightarrow \infty$ while holding the density constant[22].

The ground state solution for this Hamiltonian is[22]

$$\psi \propto \exp\left(-\frac{1}{2}\omega \sum_{i=1}^N x_i^2\right) \prod_{i<j} |x_i - x_j|^\lambda, \quad (1.19)$$

where $\lambda^2 - \lambda = \frac{1}{2}A$.

Since, for each ordering of particles, ψ is nodeless, it is the ground state wave function. ψ can be rewritten in terms of the variables

$$y_i = (\omega/\lambda)^{\frac{1}{2}} x_i \quad (1.20)$$

$$\psi = C^{\frac{1}{2}} \exp\left(-\frac{1}{2}\lambda \sum_i y_i^2\right) \prod_{i<j} |y_i - y_j|^\lambda, \quad (1.21)$$

$$\psi^2 = C \exp\left(-\frac{1}{2}\varrho \sum_i y_i^2\right) \prod_{i<j} |y_i - y_j|^\varrho, \quad (1.22)$$

with

$$\varrho = 2\lambda = 1 + (1 + 2\dot{A})^{\frac{1}{2}}. \quad (1.23)$$

C is a normalization constant, so that

$$C^{-1} = \int_{-\infty}^{\infty} \dots \int_{-\infty}^{\infty} dy_1 \dots dy_N \psi^2. \quad (1.24)$$

The ground state density ψ^2 is exactly the same as the joint probability distribution density function $P_{N\varrho}$ for the eigenvalues of matrices from a Gaussian ensemble. Choosing $\varrho = 1, 2,$ and 4 corresponds to orthogonal, unitary, and symplectic ensembles, respectively. Here, the attractive case $\dot{A} = -1/2$ corresponds to $\varrho = 1$; free fermions correspond to $\varrho = 2$.

The probability distributions of the fermion positions are exactly the same as the probability distribution of the eigenvalues in the random matrix cases. What we are interested in is the nearest-neighbor spacing distribution, which is well approximated by the Wigner surmise for the random matrix cases [19]. Since the probability distributions for the fermions and the random matrix cases are the same, the Wigner surmise applies to the spinless fermions also. However, this correspondence is justified only for the three special values of ϱ . From now on in this paper this distribution will be referred as the Wigner distribution. What we would like to do is generalize this for any values of ϱ . This distribution will be called the generalized Wigner distribution.

1.2.4 Terrace width distribution

The Schrödinger equation for the steps on a vicinal surface is [15]

$$-\frac{b^2}{2a_{\parallel}} \frac{d^2 \psi_s}{dx^2} + \frac{V}{kT} \psi_s = E_s \psi_s, \quad (1.25)$$

where b^2 is the diffusivity.

Rearranging the terms and taking the potential V to be A/x^2 type, the Hamiltonian for the whole set of steps will be

$$-\sum_i \frac{d^2}{dx_i^2} + \prod_{i < j} \frac{2\tilde{A}}{(x_i - x_j)^2}, \quad (1.26)$$

where $\tilde{A} = \frac{A}{(kT)^2} \tilde{\beta}$ and the stiffness $\tilde{\beta} = \frac{kT a_{\parallel}}{b^2}$.

Comparing this with the case of the fermions the coefficient $2\tilde{A}$ corresponds to \tilde{A} .

Substituting $2\tilde{A}$ in place of \tilde{A} in the equation (1.23) gives,

$$\varrho = 1 + (1 + 4\tilde{A})^{\frac{1}{2}}. \quad (1.27)$$

or

$$\tilde{A} = \frac{\varrho}{2} \left(\frac{\varrho}{2} - 1 \right). \quad (1.28)$$

The nearest-neighbor spacing in the fermions corresponds to the width of a terrace on the vicinal surface and the terrace width distribution is given by Wigner's approximation (equations (1.16) and (1.17)). The variance for this distribution is given by

$$\sigma^2 = \frac{\varrho + 1}{2b_\varrho} - 1. \quad (1.29)$$

In the next chapter we use Monte Carlo simulation to measure the variance of the terrace width distribution for different values of \tilde{A} and compare them with the corresponding value of the generalized Wigner surmise.

Chapter 2

Monte Carlo Simulation - Terrace Width Distribution

In all the preceding discussion, the system is assumed to be continuous along the step (y-direction) and discrete along the normal to the step (x-direction). In this Monte Carlo study, the Terrace-Step-Kink (TSK) model is used. As is shown in the figure below, the surface is discrete in both directions. For simplicity a vicinal simple cubic lattice with unit lattice constant is considered.

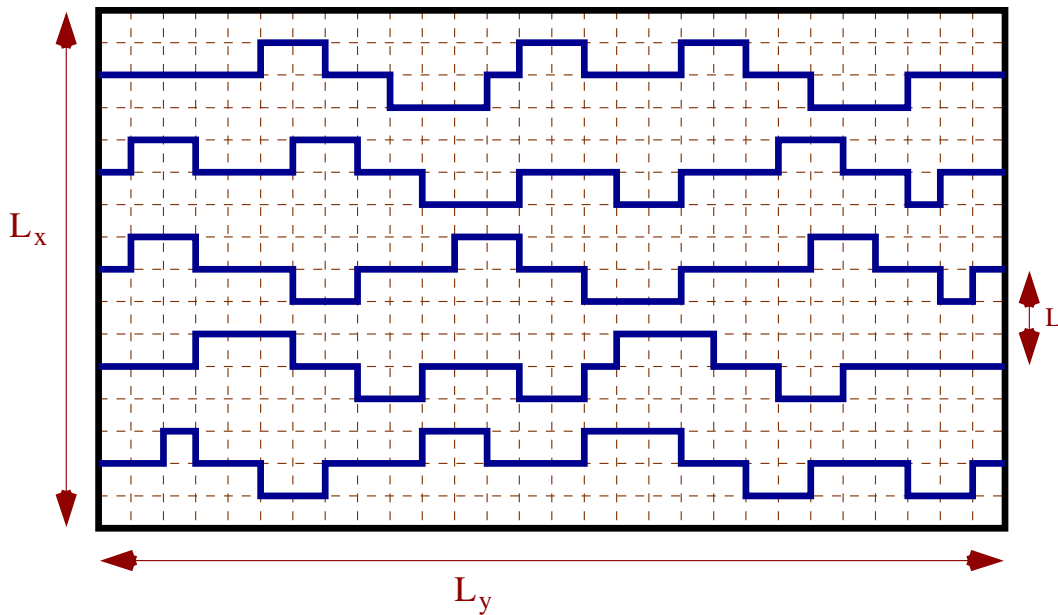


Figure 2.1: Top view of a typical surface discrete both in the x- and y-direction.

The surface is specified by the number of steps N , the length L_y along the steps and the average terrace width L . Assuming steps are of single height, the

miscut angle ϕ is related to the average terrace width by $\tan(\phi) = 1/L$. The size of the surface perpendicular to the step direction is $L_x = NL$. The position of n th step, relative to its mean position, is written as $x_n(y)$. In the TSK model the only thermal excitation is kinks of energy ϵ along the steps: the terraces have no adatoms or vacancies. Then $x_n(y)$ must be a single-valued function and the Hamiltonian contains term $\epsilon|x_n(y+1) - x_n(y)|$. The stiffness $\tilde{\beta}_{TSK}$ of an isolated step is $2k_B T \sinh^2(\epsilon/2k_B T)$ [16]. The steps are not allowed to cross, and this non-crossing constraint requires $x_{n+1}(y) > x_n(y)$.

The simulation was done by starting from straight steps. As a result of the no-crossing condition, there is an entropic repulsion between the steps. In addition there is elastic or dipole type interactions whose energies are proportional to the inverse of the square of the separation between the steps: $A/[x_{n+1}(y) - x_n(y)]^2$ [14]. Periodic boundary conditions in the y-direction and screw-periodic boundary conditions in the x-direction were used.

The goal is to measure the variance of the terrace-width distribution (TWD) for several values of \tilde{A} and compare them with what one expects from the generalized Wigner distribution results.

In order to check how the variance σ^2 changes with time, a preliminary test run was done for one of the three symmetric cases i.e. $\tilde{A} = 2$. The temperature was set to $k_B T = 0.5$ in units of the kink energy ϵ , so that the dynamics is reasonably rapid. At this temperature the stiffness $\tilde{\beta}$ is 1.1752 per lattice spacing. The lattice size is chosen with step length $L_y = 90$, number of steps $N = 10$, and the average terrace width $L = 10$. The random number generator ‘‘Ran3’’ from Numerical Recipes was

used [23]. To smooth out the fluctuations, the calculation was averaged over the 100 configurations found by different seeds. As shown in figure 2.2, a well equilibrated and smoothly varying variance could be measured.

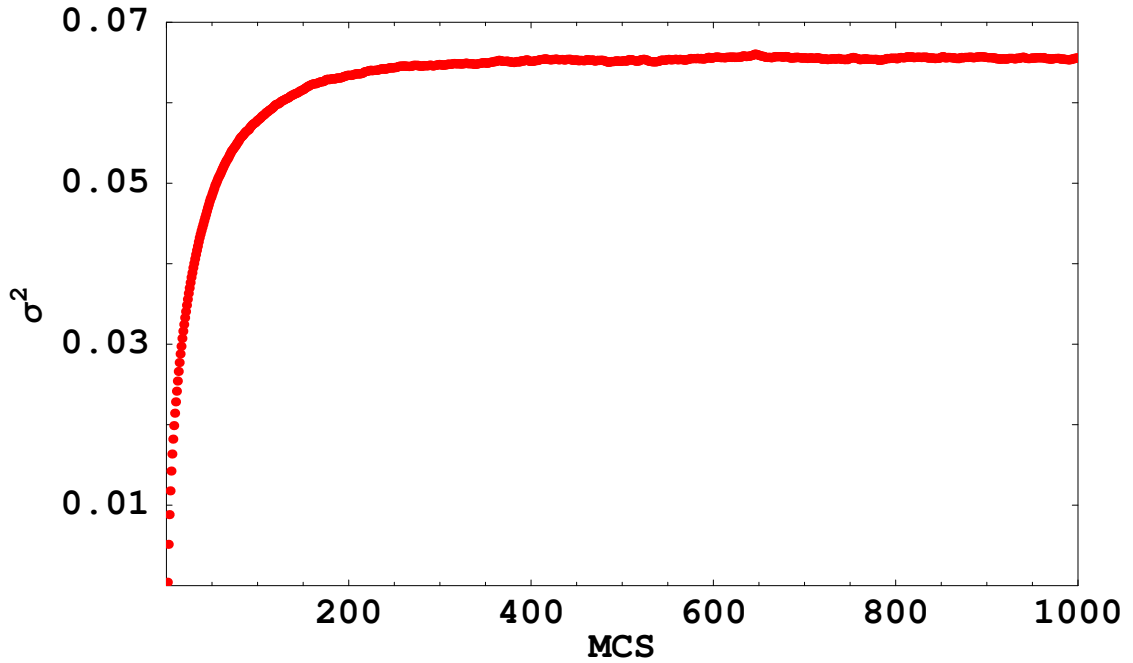


Figure 2.2: Typical plot of variance as a function of the Monte Carlo steps per site (MCS)

The size of the lattice chosen determines the equilibrium value of the variance. In order to determine the appropriate size of the lattice which gives a variance close to an expected value from the generalized Wigner distribution, calculations were done by varying the step length L_y and keeping all other parameters fixed. If one keeps on increasing the step length, the equilibrium value of the variance measured increases until it reaches the exact value. Here we do not know what the exact value is. The Wigner distribution gives a good approximation. Therefore, the difference

between the Wigner expected value and the measured variance should go to zero as L_y increases. In the next figure, the log-log plot of the difference between the measured value and the expected Wigner variance versus L_y is shown. It looks like it follows a power law of the following form:

$$\sigma_w^2 - \sigma_{MC}^2 = \frac{B}{(L_y)^\alpha}$$

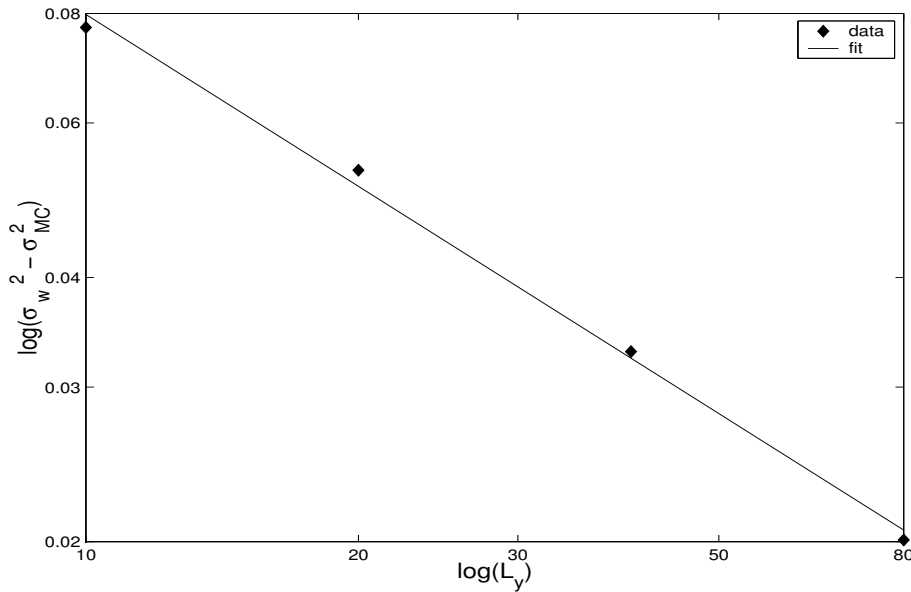


Figure 2.3: A linear fit with a log-log plot.

From the fit, B was found to be 0.36 and $\alpha = 0.65$. Using this result one can approximate how large L_y should be for a certain accuracy in σ^2 . This fitting is biased in the sense that the actual variance is assumed to be the variance from the generalized Wigner's distribution. But that presents a problem because the generalized Wigner formula is an approximation and it assumes that all steps interact,

whereas the simulation was done for just nearest neighbor interaction. To check if this bias has great effect, nonlinear fitting was done by assuming the analytical variance as one of the free parameters. The values found for B and α were very close to those found before, and the free parameter representing the variance deviates from the Wigner value by 0.001. All of this was done to get an idea how large the system had to be before it reached to a saturated value close to what we get from the generalized Wigner distribution. However, since it also depends on N and L_y , a detailed study is needed to find out how it varies with these parameters.

Monte Carlo measurements were done for different values of N and L_y . Although a simple function which describes how σ^2 varies with N and L_y could not be found, the figure below shows that the variance grows differently with L_y than it does with N .

This dependence might be different for different \tilde{A} 's. After several test runs, $L_y = 3000$, $N = 200$ and $L = 10$ were chosen for $\tilde{A} = 50$, where the difference between the measured variance and the Wigner value was found to be around 0.001. In the case when $\tilde{A} = 40$, the size was lowered to $L_y = 2000$ and $N = 100$ and the variance could be measured with the same "accuracy". The size was kept the same and the variance was measured by varying \tilde{A} .

In order to make the measured values statistically independent so errors could be calculated, the measurement was recorded in intervals of 1000 sweeps and averaged over. The calculated errors are in the order of 0.001, so small that they are

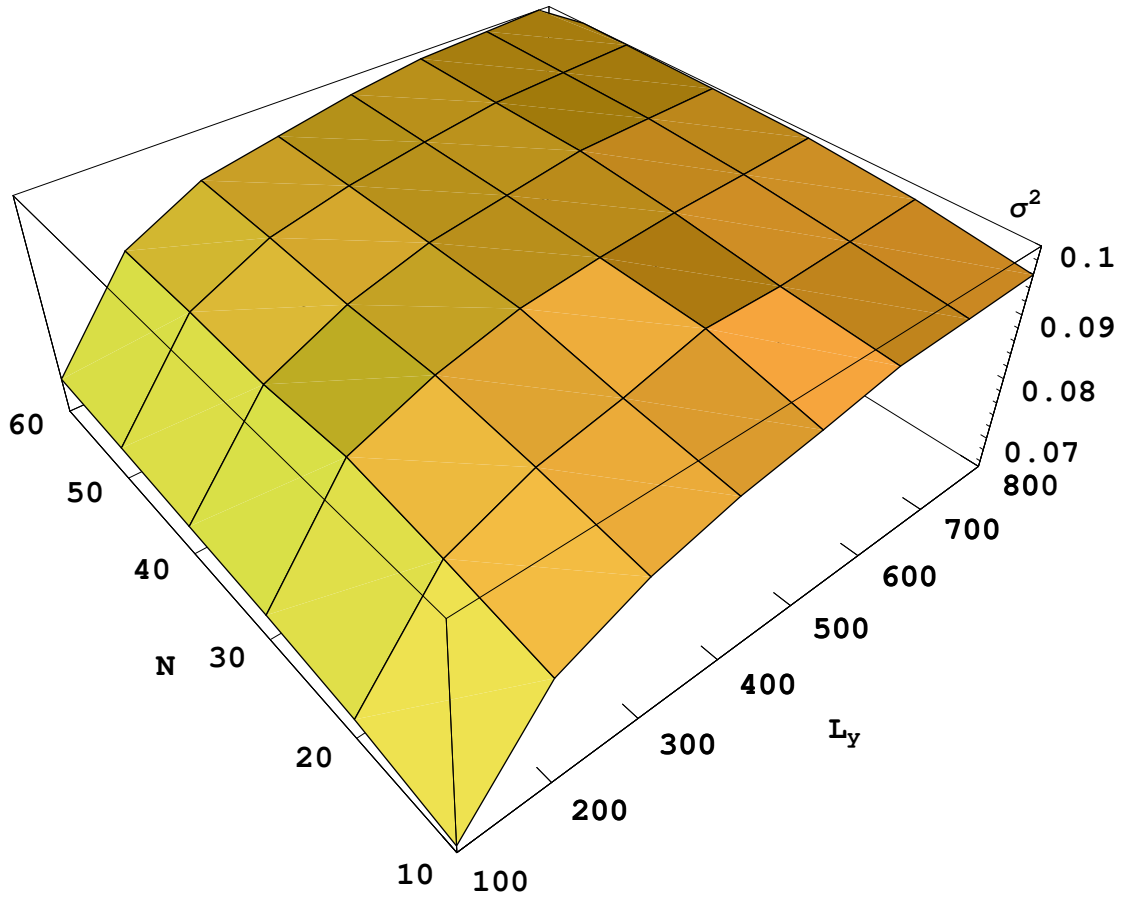


Figure 2.4: The measured variance as a function of the number of steps N and step length L_y .

not shown on the graph.

The results shown in the figure 2.5(a) below show that the measured value of the variances are very close to what one expects from the Generalized Wigner distribution . The modification of the Grenoble group gives $\sigma^2 \propto 1/\varrho$, so that a graph of $\varrho\sigma^2$ vs \tilde{A} is a horizontal line. Such a graph is shown in figure 2.5(b) where the differences among the other approximation can also be seen clearly.

The results from the Monte Carlo simulation are close to the generalized Wigner distribution, but for larger \tilde{A} the disagreement gets worse.

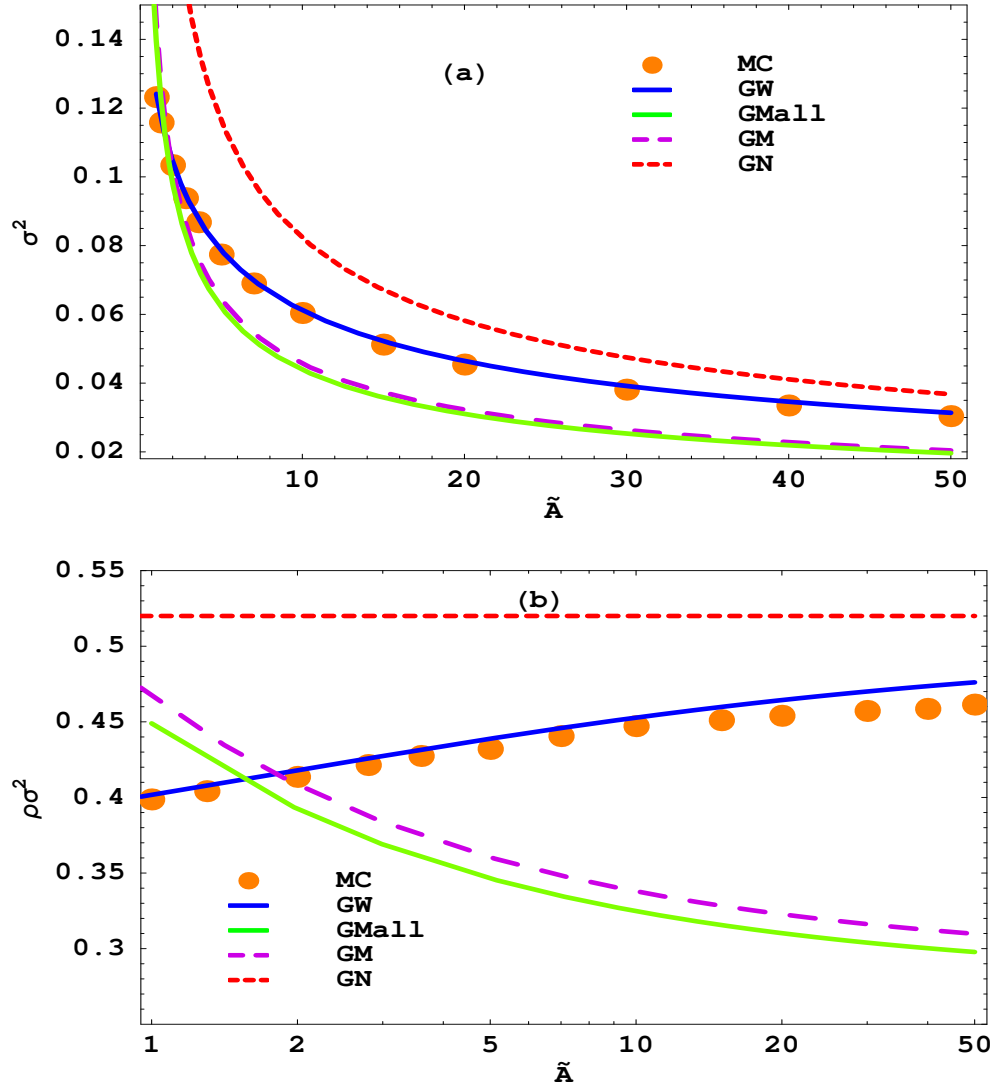


Figure 2.5: Comparison of the measured value of the variances (MC) with the expected values from the generalized Wigner distribution(GW), Gruber-Mullins with nearest neighbor interaction(GMN), Gruber Mullins with all steps interaction(GMA) and the Grenoble's group modification(GN). (a) σ^2 vs \tilde{A} ; (b) $\rho\sigma^2$ vs \tilde{A} .

Chapter 3

Fokker-Planck Derivation of Evolution of Terrace-width Distribution

3.1 Motivation

Vicinal crystals, i.e. crystals misoriented from a high-symmetry plane, have great technological importance as growth templates with controlled step “defects”. Although these steps stay in an average constant direction they are known to fluctuate. Their fluctuations give rise to a probabilistic distribution of the inter-step distance.

As we have discussed in the first two chapters the probability of finding neighboring steps at a specified separation, i.e. the terrace-width distribution (TWD), denoted by $P(s)$, where s is inter-step spacing w divided by its average value $\langle w \rangle$, has been successfully approximated by generalized Wigner surmise.

$$P_\varrho(s) = a_\varrho s^\varrho \exp[-b_\varrho s^2], \quad (3.1)$$

where

$$b_\varrho = \left[\frac{\Gamma\left(\frac{\varrho+2}{2}\right)}{\Gamma\left(\frac{\varrho+1}{2}\right)} \right]^2 \quad \text{and} \quad a_\varrho = \frac{2b_\varrho^{(\varrho+1)/2}}{\Gamma\left(\frac{\varrho+1}{2}\right)} \quad (3.2)$$

assure the normalization and unit mean $\langle s \rangle = 1$. Using the correspondence with the Calogero-Sutherland model of 1D interacting fermion model, the dimensionless

interaction strength $\tilde{A} = A\tilde{\beta}/(k_B T)^2$ is related to ϱ by

$$\tilde{A} = \frac{\varrho}{2} \left(\frac{\varrho}{2} - 1 \right). \quad (3.3)$$

Both in numerical simulations and in actual experiments, the probability distribution in equation 3.1 gives a better accounting of the TWD than any of the preexisting Gaussian model [17, 31]. However, there is no symmetry argument such as used by Wigner to justify the form of equation (3.1) for a general value of the interaction strength. In this chapter a comprehensive derivation of the generalized Wigner surmise is presented. Moreover, this Fokker-Planck approach provides a description of how experimentally relevant non-equilibrium TWDs evolve toward the steady-state Wigner form.

3.2 The Fokker-Planck Derivation

We start with Dyson's Brownian motion model [20]. It is based on the analogy drawn by Dyson between Random Matrix Theory (RMT) and a Coulomb gas model [32], namely a "gas" of N particles on a line, interacting with a logarithmic potential, and confined by a harmonic potential. The Coulomb gas model helps understanding the fluctuation properties of the spectrum of complex conserved systems. Slightly broken symmetries act as perturbations on the conserved properties, and can be accounted for by a dynamic model, the Brownian motion, model, in which the N particles are subject, besides the mutual repulsions, to dissipative forces [20]. The particle positions x_i then obey the Langevin equations,

$$\dot{x}_i = -\gamma x_i + \sum_{i \neq j} \frac{\hat{\rho}}{x_i - x_j} + \sqrt{\Gamma} \eta \quad (3.4)$$

where η is a delta-correlated white noise and $\hat{\rho}$ ($\propto \rho$) is the “charge” of each particle.

This Langevin equation can be written as the deterministic and the noise part,

$$\dot{x}_i = F(x_i) + \sqrt{\Gamma} \eta \quad (3.5)$$

The first two terms on the right hand side of equation 3.4 represent the deterministic part of the force acting on the i^{th} particle,

$$F(x_i) = -\gamma x_i - \sum_{k>i} \frac{\hat{\rho}}{x_k - x_i} + \sum_{i>q} \frac{\hat{\rho}}{x_i - x_q}, \quad (3.6)$$

Similarly, we can write equation (3.5) for the $(i+1)^{\text{th}}$ particle as

$$\dot{x}_{i+1} = F(x_{i+1}) + \sqrt{\Gamma} \eta, \quad (3.7)$$

where the deterministic part of the force acting on the $(i+1)^{\text{th}}$ particle is given by

$$F(x_{i+1}) = -\gamma x_{i+1} - \sum_{k>(i+1)} \frac{\hat{\rho}}{x_k - x_{i+1}} + \sum_{(i+1)>q} \frac{\hat{\rho}}{x_{i+1} - x_q}. \quad (3.8)$$

We are interested to find an equation for the separation between particles $w_i \equiv x_{i+1} - x_i$. If we subtract equation 3.5 from equation 3.7, we get

$$\dot{w}_i = F(x_{i+1}) - F(x_i) + \sqrt{2\Gamma} \eta \quad (3.9)$$

where

$$F(x_{i+1}) - F(x_i) = \left(-\gamma x_{i+1} - \sum_{k>(i+1)} \frac{\hat{\theta}}{x_k - x_{i+1}} + \sum_{(i+1)>q} \frac{\hat{\theta}}{x_{i+1} - x_q} \right) - \left(-\gamma x_i - \sum_{k>i} \frac{\hat{\theta}}{x_k - x_i} + \sum_{i>q} \frac{\hat{\theta}}{x_i - x_q} \right) \quad (3.10)$$

Rearranging terms so that the terms containing only $x_{i+1} - x_i = w_i$ are separated from the others, we find

$$F(x_{i+1}) - F(x_i) = -\gamma(x_{i+1} - x_i) - \hat{\theta} \left[\frac{-2}{x_{i+1} - x_i} + \sum_{k>i+1} \left(\frac{1}{x_k - x_i} - \frac{1}{x_k - x_{i+1}} \right) + \sum_{i>q} \left(\frac{1}{x_{i+1} - x_q} - \frac{1}{x_i - x_q} \right) \right]$$

The last two terms can be rewritten as follows

$$\sum_{k>i+1} \frac{x_{i+1} - x_i}{(x_k - x_{i+1})(x_k - x_i)} + \sum_{i>q} \frac{x_{i+1} - x_i}{(x_{i+1} - x_q)(x_i - x_q)} \quad (3.11)$$

In order to further decouple the force dependence on w_i from the other variables, we assume, in a mean field spirit, that the denominators $(x_k - x_{i+1})(x_k - x_i)$ in equation (3.11) are replaced by their mean values, the average being taken in the stationary state:

$$\langle (x_k - x_{i+1})(x_k - x_i) \rangle_{st} = \langle w^2 \rangle (k - i - 1)(k - i). \quad (3.12)$$

Letting $k - i = p$, $q - i = r$, the sums in Eq.(3.11) simplify greatly to

$$\frac{x_{i+1} - x_i}{\langle w^2 \rangle_{st}} \left[\sum_{p>0} \frac{1}{(p+1)p} + \sum_{r>0} \frac{1}{(r+1)r} \right] \quad (3.13)$$

where each of the two terms is unity. The Langevin equation for the terrace-width is (dropping the index),

$$\dot{w} = -2 \left[\left(\frac{\gamma}{2} + \frac{\hat{\rho}}{\langle w^2 \rangle_{st}} \right) w - \frac{\hat{\rho}}{w} \right] + \sqrt{2\Gamma} \eta. \quad (3.14)$$

The above equation is called a Rayleigh process [39, 40] if $\sqrt{2\Gamma} = \hat{\rho}$. The goal is to convert the Eq.(3.14) into a Fokker-Planck equation with the generalized Wigner TWD as its steady-state solution. Using the formula given in ref.[39] the corresponding Fokker-Planck equation is given by

$$\frac{\partial P(w, t)}{\partial t} = \frac{\partial}{\partial w} \left\{ \left[\left(\gamma + \frac{2\hat{\rho}}{\langle w^2 \rangle} \right) w - \frac{2\hat{\rho}}{w} \right] P(w, t) \right\} + \Gamma \frac{\partial^2 P(w, t)}{\partial w^2} \quad (3.15)$$

Treating γ as a self-consistency parameter and recognizing $2\hat{\rho} = \rho\Gamma$, we set $\gamma = \Gamma/\langle w^2 \rangle$. The Fokker-Planck equation then becomes

$$\frac{\partial P(w, t)}{\partial t} = \frac{\partial}{\partial w} \left\{ \left[\left(\frac{(\rho + 1)\Gamma}{\langle w^2 \rangle} \right) w - \frac{2\hat{\rho}}{w} \right] P(w, t) \right\} + \Gamma \frac{\partial^2 P(w, t)}{\partial w^2} \quad (3.16)$$

For a dimensionless variable $s \equiv w/\langle w \rangle_{st}$, we know from Wigner's distribution that $\langle s^2 \rangle = (\rho + 1)/2b_\rho$ [4, 20]. Changing to the dimensionless variable s and $\tilde{t} = \Gamma t/\langle w \rangle^2$, the sought-after Fokker-Planck equation is

$$\frac{\partial P(s, \tilde{t})}{\partial \tilde{t}} = \frac{\partial}{\partial s} \left[\left(2b_\rho s - \frac{\rho}{s} \right) P(s, \tilde{t}) \right] + \frac{\partial^2}{\partial s^2} [P(s, \tilde{t})]. \quad (3.17)$$

To solve Eq.(3.17) we must specify the initial distribution in s_0 . Stratonovich [40] proceeds by separation of variables, finding the spatial eigenfunctions in terms

of Laguerre polynomials. After some manipulation, we then find the distribution in s at rescaled time \tilde{t} , given an initial sharp distribution $\delta(s - s_0)$, to be

$$P(s, \tilde{t}|s_0) = 2\tilde{b}_\varrho \frac{s^{\alpha+1}}{\tilde{s}_0^\alpha} I_\alpha \left(2\tilde{b}_\varrho s \tilde{s}_0 \right) \exp \left[-\tilde{b}_\varrho \left(s^2 + \tilde{s}_0^2 \right) \right] \quad (3.18)$$

where $\alpha = (\varrho - 1)/2$, $\tilde{b}_\varrho \equiv b_\varrho / (1 - e^{-\tilde{t}})$, $\tilde{s}_0 \equiv s_0 \exp(-\tilde{t}/2)$, and I_α is the modified Bessel function of the first kind.

At long enough time the variable \tilde{s}_0 goes to zero while \tilde{b}_ϱ and s remain finite. Using the limiting value $I_\alpha(x) \sim (x/2)^\alpha / \Gamma(\alpha + 1)$ as $x \rightarrow 0$ and the definitions in Eq.(3.2), we find

$$P(s, \tilde{t}) \sim \frac{a_\varrho s^\varrho}{(1 - e^{-\tilde{t}})^{(\varrho+1)/2}} \exp \left[-s^2 b_\varrho / (1 - e^{-\tilde{t}}) \right], \quad (3.19)$$

confirming that at long enough times \tilde{t} , any dependence on s_0 disappears and that Eq.(3.19) approaches Eq.(3.1). Now we consider three experimentally interesting situations with special initial distributions.

1. Perfectly cleaved crystals:

The first one is a perfectly cleaved crystal which is used for the Monte Carlo Simulation. In this case the initial distribution is given by a delta function at the mean spacing, i.e $\delta(s_0 - 1)$, and the solution Eq.(3.18) reduces to

$$P(s, \tilde{t}) = 2\tilde{b}_\varrho s^{\alpha+1} e^{\alpha\tilde{t}/2} I_\alpha \left(2\tilde{b}_\varrho s e^{-\tilde{t}/2} \right) \exp \left[-\tilde{b}_\varrho \left(s^2 + e^{-\tilde{t}} \right) \right] \quad (3.20)$$

In experimental works, $P(s)$ is generally characterized by its variance(σ^2).

For the solution in Eq.(3.20) it can be calculated from its first and second moments, μ_1 and μ_2 . The first and second moment are calculated to be

$$\mu_1 = \frac{\sqrt{1 - e^{-\tilde{t}}} {}_1F_1\left(\frac{\varrho+2}{2}, \frac{\varrho+1}{2}, \tilde{b}_\varrho e^{-\tilde{t}}\right)}{\exp\left(\tilde{b}_\varrho e^{-\tilde{t}}\right)} \quad \text{and} \quad \mu_2 = \left[\frac{(\varrho+1)}{(2\tilde{b}_\varrho)}\right] + e^{-\tilde{t}} \quad (3.21)$$

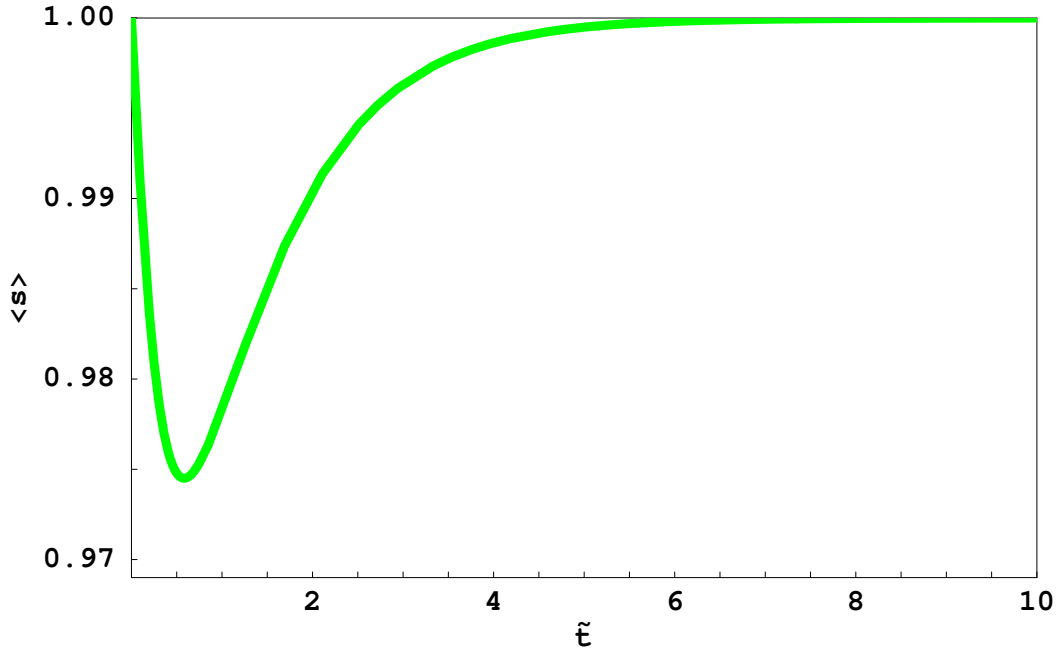


Figure 3.1: The graph of first moment predicted using the Fokker-Planck analytical prediction for an initially perfectly-cleaved crystal with $\tilde{A} = 0$, $\varrho = 2$.

The graph in figure(3.1) shows that the first moment varies with time in a non-trivial manner. This behavior is perhaps attributable to the mean-field like approximation made in the derivation of the Fokker-Planck equation. One should note that the dip in the graph is very small, so that one can take the first moment as $\mu_1 = 1$. The variance is then given by

$$\sigma^2(\tilde{t}) = \sigma_\infty^2 (1 - e^{-\tilde{t}}), \quad (3.22)$$

where $\sigma_\infty^2 = \langle s^2 \rangle - 1 = [(\varrho + 1) / 2b_\varrho] - 1$.

This is compared with the results of Monte Carlo Simulation shown on fig(3.2).

As discussed in the previous chapter, the terrace-step-kink model is used with $A = 0$ (just entropic interaction), setting $k_B T$ to half of the kink energy, with 4 steps, 200 spacings in length, and $\langle w \rangle = 6$. To compare the simulation with the Fokker-Planck analytic prediction, we manually set the time scale of the simulation to get the best match of the dimensionless \tilde{t} : 10^3 MCS corresponds to 1.4 units of \tilde{t} . As shown in the fig(3.2) the agreement is remarkably good.

Keeping everything else the same, we next took $A = 0.5$, which corresponds to $\tilde{A} = 2.762$ at this T . In this case, we find that to get good agreement between simulation and prediction, 10^3 MCS corresponds to 4.5 units of \tilde{t} .

2. Step bunch:

In this case the initial distribution is a delta function around a vanishing terrace size, $P(s_0, 0) = \delta(s_0)$. Experimentally, this situation may be easier to realize, for instance by inducing the formation of a bunch of steps (step bunching), and then watching the steps spread out to their equilibrium arrangement. The full time-dependent solution is found to be the same as Eq. (3.19). In this case, the experimental terrace-width-distribution should have

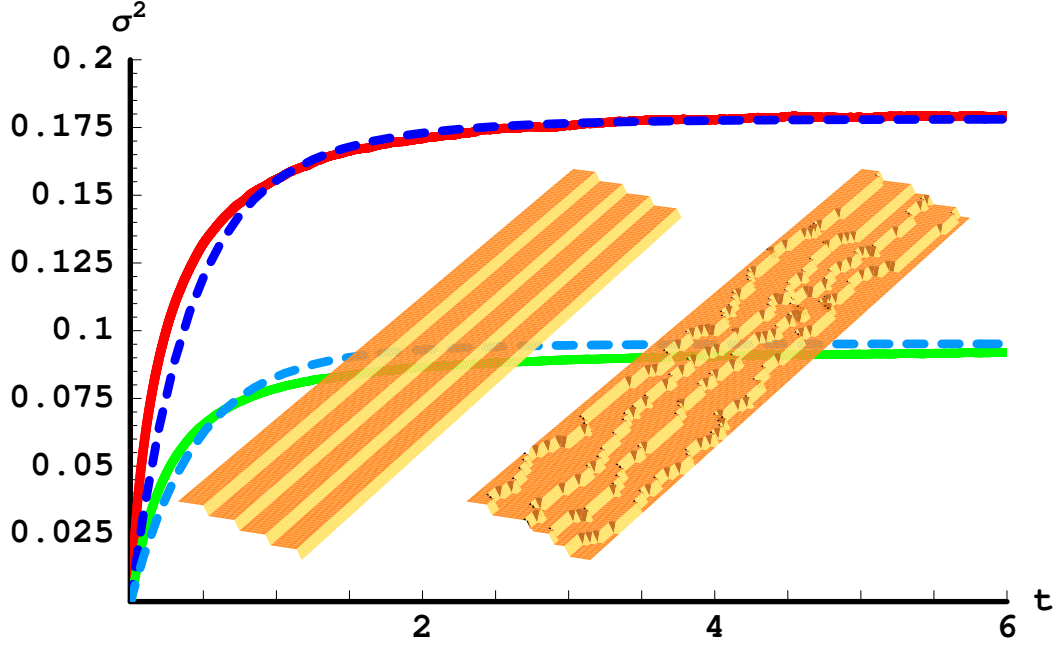


Figure 3.2: Comparison of the variance predicted using the Fokker-Plank analytical prediction(dashed lines) and the variance computed using conventional Metropolis Monte-Carlo for a terrace-step-kink model(solid lines). The upper curves are for “free fermions” ($\tilde{A} = 0$, $\varrho = 2$). Both upper curves approach the equilibrium variance $\sigma_{\infty}^2 = 0.18$ [4]. The lower pair of curves show the predicted(dashed) and computed (solid) variances for $\tilde{A} \approx 2.762$, $\varrho \approx 4.47$, with a different scaling factor between \tilde{t} and MC time. Both lower curves approach $\sigma_{\infty}^2 = 0.095$. The left and right inset panels show the initial and a typical late-time configuration of the steps in the Monte Carlo simulation, respectively.

a first moment that increases rapidly from its initial value to unity according to $\mu_1 = \sqrt{1 - e^{-\tilde{t}}}$. The variance of Eq.(3.19) approaches the equilibrium value as $\sigma^2 = \sigma_{\infty}^2 (1 - e^{-\tilde{t}})$, where the Wigner variance σ_W^2 is given by

$$\sigma_W^2 + 1 = (\varrho + 1) / 2b_\varrho.$$

3. Quenches:

The third physically interesting case is what is called quenching (or upquenching). This is the case where a system has attained equilibrium at one temperature and suddenly subjected to a different temperature. In this problem that amounts to a sudden change from ϱ_0 to ϱ . The probability distribution $P(s, \tilde{t})$ is obtained by integrating Eq.(3.18) weighted by the equilibrium distribution $P_{\varrho_0}(s_0)$. After some manipulation we found

$$P(s, \tilde{t}) = a_\varrho s^\varrho e^{-\tilde{b}_\varrho s^2} \frac{(1 - e^{-\tilde{t}})^{\frac{\varrho_0 - \varrho}{2}}}{(1 - e^{-\tilde{t}} (1 - b_\varrho / b_{\varrho_0}))^{\frac{\varrho_0 + 1}{2}}} \times {}_1F_1 \left(\frac{\varrho_0 + 1}{2}, \frac{\varrho + 1}{2}, \frac{\tilde{b}_\varrho s^2}{1 + (b_{\varrho_0} / b_\varrho) (e^{\tilde{t}} - 1)} \right). \quad (3.23)$$

with ${}_1F_1$ the Kummer confluent hypergeometric function. This solution satisfies the following necessary conditions. For $\varrho_0 = \varrho$, it reduces to Eq.(3.1), since ${}_1F_1(a, a, z) = \exp(z)$. For asymptotically large ϱ_0 Eq.(3.23) reduces to Eq.(3.20). For arbitrary ϱ_0 and ϱ , it is initially $P_{\varrho_0}(s)$ and approaches $P_\varrho(s)$ at long times. We are able to compute the first and second moments for this general case and they are given by

$$\mu_1 = \tilde{b}_\varrho^{-1/2} \left(1 - \frac{e^{-\tilde{t}}}{1 + \frac{b_{\varrho_0}}{b_\varrho} (1 - e^{-\tilde{t}})} \right)^{\frac{\varrho_0 + 1}{2}} \times$$

$$\mu_2 = \frac{{}_2F_1\left(\frac{\varrho+2}{2}, \frac{\varrho_0+1}{2}, \frac{\varrho+1}{2}, \left[1 + \frac{b_{\varrho_0}}{b_{\varrho}}(e^{\tilde{t}} - 1)\right]^{-1}\right)}{2\left(1 + \frac{b_{\varrho}}{b_{\varrho_0}}\right)\tilde{b}_{\varrho}} \left(\varrho + \frac{1+b_{\varrho_0}e^{-\tilde{t}}}{1-e^{-\tilde{t}}}\right) \quad (3.24)$$

This formulation not only places the generalized Wigner on firmer theoretical ground, it allows the exploration of the evolution of TWDs as a whole rather than just positions of individual steps.

Chapter 4

Stochastic description of fluctuating steps

4.1 Motivation

There are a lot of attempts to use the idea of equilibrium statistical mechanics to explain how a surface evolves after it reaches at its thermodynamic equilibrium. As steps are the fundamental entities, the evolution of a vicinal surface toward and/or at equilibrium can be described by following the position of steps through time. Theoretically this is done by using a model to write equation of motion for points on each step. Since the ultimate goal here is to understand the equilibrium properties of surfaces, whatever motion is observed should be due to thermal fluctuations which are stochastic by nature. These stochastic motions are well described by Langevin formalism. In this chapter a review of known properties of step fluctuations is presented. In the first section, the Langevin formalism is reviewed. Next, properties of quantities like width, correlations, persistence and survival probabilities are discussed, both as predicted by the theory and observed in the experiments.

4.2 Langevin Formalism

The Langevin approach is widely used for the purpose of finding the effect of fluctuations in macroscopically known systems. In our special case of step or inter-

face evolution, we are able to model step fluctuation using the Langevin formalism without trying to incorporate the details of the atomic scale transport processes. In general fluctuations are introduced in the Langevin equation by adding random terms to the equation of motion. Here the random nature of the atomic-scale processes are represented by a noise term introduced in a stochastic Langevin equation.

$$\partial_t x(y, t) = f[x(y, t)] + \eta(y, t) \quad (4.1)$$

where $x(y, t)$ is the position of a step at point y along the step at time t and $\eta(y, t)$ represents the noise taking care of the stochastic nature of the motion. The amplitude and correlations of the noise term are determined by the process under consideration. The functional f describes the atomistic limiting process responsible for the motion of the step, and its form is determined by symmetries of the processes involved.

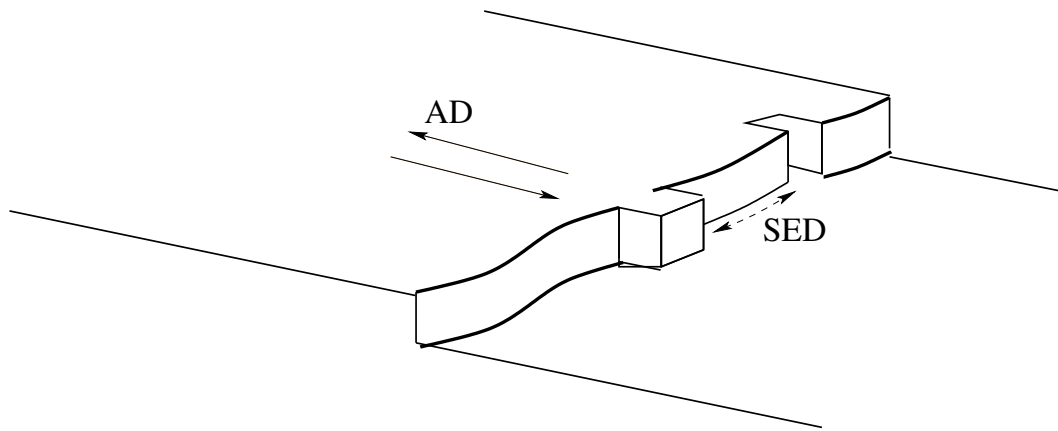


Figure 4.1: Schematic diagram of the two common limiting processes: Attachment-Detachment (AD) and Step-Edge-Diffusion limiting processes.

There are two common limiting processes modeled by the Langevin equation [2, 3, 24, 25, 26, 27, 28]. They are referred as attachment-detachment (AD) and step-edge diffusion (SED) limiting processes. As is shown in the schematic diagram (figure (4.1)), AD is a process where the steps fluctuate because of the random exchange of mass between the step and its adjacent terrace. Microscopically, this process involves atoms on the step edge attach and detach surpassing the energy barrier for the particular process. The deterministic part $f[x(y, t)]$ of the Langevin equation 4.1 for this process is governed by the free energy change associated with step displacement and is written by substituting it with a functional derivative of the free energy.

$$\partial_t x(y, t) = -\frac{\Gamma_a}{k_B T} \frac{\delta F}{\delta x} + \eta(y, t) \quad (4.2)$$

Here the analog of a friction coefficient, Γ_a , called the step attachment/detachment mobility, is introduced. It is one of the key measurable linear kinetic parameter governing the AD process [3]. The free energy functional F in equation 4.2 takes the form [29]

$$F = \int \frac{\tilde{\beta}}{2} (\partial_y x)^2 dy \quad (4.3)$$

where $\tilde{\beta}$ is the second measurable quantity called the stiffness of the step. It is defined as the sum of the energy per unit length and its second derivative with respect to the angle the steps forms with a high symmetry direction of the step, $\tilde{\beta} = \beta + \frac{\partial^2 \beta}{\partial \theta^2}$. If we do the functional derivative in equation 4.2, the resulting stochastic

linear partial differential equation describes the AD limiting process fluctuation of an isolated step.

$$\frac{\partial x(y, t)}{\partial t} = \frac{\Gamma_a \tilde{\beta}}{k_B T} \left(\frac{\partial^2 x}{\partial y^2} \right) + \eta(y, t) \quad (4.4)$$

This equation provides exactly solvable model for the AD process that can be used to calculate experimentally measurable quantities. In AD process the noise is referred to as white noise or uncorrelated in both space and time and has zero mean [29, 30].

$$\langle \eta(y, t) \eta(y', t') \rangle = D \delta(y - y') \delta(t - t') \quad (4.5)$$

The noise magnitude D is a constant related to the other phenomenological parameters introduced. The *Fluctuation Dissipation Theorem* relates dissipative transport coefficients to the autocorrelation function of a noise term [34, 35]. In the case of AD limited kinetics of step edge fluctuation, the noise magnitude is related to the step mobility simply by $D = 2\Gamma_a$ [29]. Thus, near-equilibrium structure and dynamics of steps in the limiting case of this simple transport process is modeled using only two parameters. One of them is the step mobility, which determines the kinetics of fluctuation of the step about its equilibrium position and the other one is the step stiffness, mass-like inertial parameter that governs the equilibrium step structure.

Several numerically and experimentally measurable quantities can be obtained by solving the linear stochastic equation 4.4 using the method of Fourier transform.

The stochastic equation for the Fourier components can be found by substituting equation 4.6 and by applying the same Fourier transformation to the noise term.

$$x(y, t) = \sum_q e^{iqy} x_q(t) \quad (4.6)$$

$$\partial_t x_q = -\frac{x_q}{\tau(q)} + \eta_q \quad (4.7)$$

The time constant τ_q introduced here is the characteristic time scale for relaxation of a mode of wavelength q , and it is very useful in understanding of step fluctuations. For the particular AD process, it is given by

$$\tau(q) = \frac{k_B T}{\tilde{\beta} q^2 \Gamma_a} \quad (4.8)$$

Equation 4.7 is in a simple form whose solution leads to many quantities of interest. In particular the Fourier time correlation function of a Fourier mode is very useful, and it is defined as

$$G_q(t - t') = \langle |x_q(t) - x_q(t')|^2 \rangle. \quad (4.9)$$

Solving equation 4.7 for this quantity gives

$$G_q(t - t') = \frac{2k_B T}{\tilde{\beta} q^2} \left[1 - \exp\left(\frac{-|t - t'|}{\tau(q)}\right) \right]. \quad (4.10)$$

This result is a very general formula in which the dependence of the quantity on the particular limiting process is buried in the form of $\tau(q)$. The relation $\tau(q) \propto q^{-2}$ has been used to identify for the AD-process in experimental systems. This

can be done by obtaining the position of a step using a real-space technique (e.g. STM) [33]. These configurations can be numerically decomposed into their Fourier components, one then calculates the time correlation G_q for each component and extract the time constant for decay of each component. By fitting the experimental correlation function to equation (4.10), the two measurable quantities, step stiffness and mobility, can be extracted [30, 36].

In many experimental studies of step fluctuations, the Fourier description is not feasible. Instead (in STM for example) the position of a single point on a step edge is measured, and the real space temporal correlation function

$$G(t) = \langle (x(y, t + t_0) - x(y, t_0))^2 \rangle \quad (4.11)$$

is calculated where the angular brackets is for averaging over all initial time t_0 . This quantity is found to have power law dependence on time. Exact results for specific case of AD process gives

$$G(t) = \left(\frac{4k_B T \Gamma_a t}{\pi \tilde{\beta}} \right)^{1/2} \quad (4.12)$$

This equation provides an alternative way of determining the limiting process responsible for a step fluctuation under consideration. Fitting the experimental $G(t)$ to a power law gives the combination of stiffness and step mobility. One disadvantage of this method is that one of the quantities (usually step stiffness) has to be determined from a different experimental analysis.

The other common limiting process in surface transport is the diffusion of

mass along the step edge appropriately called periphery diffusion or step-edge diffusion (SED). It can be modeled by using the same procedure as the AD process described above, but with a different relaxation functional in the Langevin equation and different correlation for the noise term. The basic distinguishing feature of SED is that, since mass is diffusing along the step edge, the number of atoms on the step must be conserved. The Langevin equation for SED is

$$\partial_t x(y, t) = \frac{\Gamma_h}{k_B T} \partial_y^2 \frac{\delta F}{\delta x} + \eta_c(y, t). \quad (4.13)$$

The negative second derivative in front of the functional derivative ensures that the relaxation term is conservative, and the noise term has the subscript c to indicate that its correlations must also enforce conservation. The new parameter Γ_h is the step-edge hopping mobility and describes the rate of mass transport along the step edge. After evaluating the functional derivative, the equation becomes

$$\partial_t x(y, t) = -\frac{\Gamma_h \tilde{\beta}}{k_B T} \frac{\partial^4 x}{\partial y^4} + \eta_c(y, t) \quad (4.14)$$

The conserved noise still has zero mean but the correlations are modified to

$$\langle \eta_c(y, t) \eta_c(y', t') \rangle = -2\Gamma_h \partial_y^2 \delta(y - y') \delta(t - t') \quad (4.15)$$

where the *Fluctuation Dissipation Theorem* has already been implemented to express noise strength in terms of the SED mobility.

The same procedure as in the AD case can be followed to calculate the correlation G_q . The result is known to be the same as before except the q dependence of

τ_q is now different

$$\tau(q) = \frac{k_B T}{\Gamma_h \tilde{\beta} q^4}. \quad (4.16)$$

This enables us to use the experimental time constants to distinguish fluctuations limited by this process from the AD process. The form of real-space temporal correlation function is also distinct for SED is given by [3, 2, 29, 37]

$$G(t) = \Gamma(3/4) \left(\frac{(k_B T)^3 \Gamma_h t}{\tilde{\beta}^3} \right)^{1/4}. \quad (4.17)$$

$G(t)$ grows much more slowly in time for SED-limited kinetics than AD-limited kinetics. The function again contains only the two key measurable parameters, stiffness and mobility. Therefore, the SED process can clearly also be modeled in the continuum step picture using the thermodynamic stiffness and the kinetic parameter, Γ_h .

On the other hand SED is a process limited by the time scale for the atoms to diffuse along the step edge. According to simple bond-counting the energy barrier for AD is higher than for SED processes. Therefore, in a particular system, AD is observed at higher temperatures than where SED is seen.

The Langevin equations for these two limits are one-dimensional versions of similar equations one encounters in growth models and different stochastic phenomena [38, 39]. In reference [38] growth models are discussed using scaling properties resulting in universality classes. For example the AD Langevin equation is exactly the same as the Edwards-Wilkinson (EW) growth equation, so both belong to the

same universality class. These classes are differentiated through exponents one obtains in the functional dependence of width and correlation functions on time and system size.

The usual starting point in analyzing growth of interfaces like steps is the scaling ansatz for the interface width (width of the fluctuations). The width of fluctuations is the quantity which measures the roughness of the step edge length L_y . It is defined by

$$W(L_y, t) = \langle (x(t) - \bar{x}(t))^2 \rangle^{1/2} \quad (4.18)$$

where $\bar{x}(t)$ denotes the average position of the step. For a step initially straight at the origin, the fluctuation width starts from zero and grows as a power law with an exponent β

$$W(L_y, t) \sim t^\beta. \quad (4.19)$$

However, for a finite length of the step, it does not increase indefinitely; rather it is followed by a saturation region where it levels off at a saturation value W_{sat} which increases with the length L_y according to

$$W_{sat}(L_y) \sim L_y^\alpha \quad (4.20)$$

where α is called roughness exponent. In particular for the EW universality class (attachment-detachment) case the exponent $\alpha = 1/2$ and the full functional form of the saturation value is [41]

$$W_{sat}^2 = \frac{k_B T L_y}{12 \tilde{\beta}}. \quad (4.21)$$

The crossover time t_x at which the step edge crosses from the behavior of Eq.(4.19) to that of (4.20) depends on the system size,

$$t_x \sim L_y^z, \quad (4.22)$$

where z is called the dynamic exponent. The three exponents are not independent; they are related by

$$z = \frac{\alpha}{\beta}. \quad (4.23)$$

In general form this is written as

$$W(L_y, t) \sim L_y^\alpha f\left(\frac{t}{L_y^z}\right). \quad (4.24)$$

Using dynamical scaling concepts, properties of the function f are determined in two regimes; they are

$$f(u) \sim \begin{cases} u^\beta & \text{for } u \ll 1 \\ \text{const} & \text{for } u \gg 1 \end{cases}$$

There is another important quantity in describing the evolution of step fluctuations. This is specially important in relation to the first passage properties. It is defined as $C(t) = \langle (x(y, t + t_0) - \bar{x}(t + t_0))(x(y, t_0) - \bar{x}(t_0)) \rangle$ where the averaging is done over different initial times t_0 and different realizations. This correlation function is not independent of the width W and time correlation function $G(t)$. For the

cases where t_0 is chosen to be in the region where the steps reached equilibrium, it is related to the width of the fluctuation and the correlation function $G(t)$ as follows [41]

$$C(t_0) = W_{sat}^2 \quad (4.25)$$

and

$$C(t) = W_{sat}^2 - \frac{1}{2}G(t) \quad (4.26)$$

Using discrete Fourier transform and considering a finite system size, the long time asymptotic behavior of the steady-state autocorrelation function is

$$C(t) = \frac{k_B T L_y}{2\pi^2 \tilde{\beta}} e^{-t/\tau_c} \quad (4.27)$$

where the correlation time is given by

$$\tau_c(L_y) = \frac{k_B T L_y^z}{(2\pi)^2 \Gamma_a \tilde{\beta}} \quad (4.28)$$

4.3 First Passage Probabilities

The statistics of first passage events in spatially extended systems have been studied theoretically ([43, 48, 50] and references therein) and experimentally [43, 45, 46, 51]. The asymptotic decay of first passage probabilities turns out to be hard to compute even for simple systems such as the linear diffusion model [52, 53]. In different systems these probabilities are defined in slightly different ways. There

are two definitions which are very similar, but careful studies have shown that they behave differently [48].

The first one is known as the persistence probability $P(t)$, defined as the probability that the stochastic variable (in our case step position) does not come back to its original value within a time interval t . It has been studied numerically and for experimental systems with known asymptotic properties of the correlations [44, 48, 50]. Depending on whether the fluctuating surface has reached at its equilibrium or not, there are two kinds of persistence probabilities: transient and steady-state, respectively. Both are found to follow power laws but with slightly different exponents [44, 50]. The transient exponent does not seem to be related to any other exponent known from growth processes or interface fluctuation. On the other hand theoretical [44, 50] and experimental [45, 46] works have shown that the steady-state exponent is related to the growth exponent β :

$$P(t) \sim t^{-\theta}, \tag{4.29}$$

where θ is the steady-state persistence exponent. It is related to the growth exponent by

$$\theta = 1 - \beta. \tag{4.30}$$

The relation of persistence and growth exponents is derived [44, 50] by using the fact that the G-correlation function $G(t, t') = \lim_{t_0 \rightarrow \infty} \langle [x(y, t+t_0) - x(y, t'+t_0)]^2 \rangle$ depends only on the time difference $|t - t'|$ (and not on the individual times t and

t') in a power law fashion for large $|t - t'|$

$$G(t, t') \sim |t - t'|^{2\beta}, \quad (4.31)$$

where β is the growth exponent.

This particular behavior of the correlation function in Eq. (4.31) is typical of fractional Brownian motion (fBm). A stochastic process $u(t)$ with zero mean is called an fBm if its incremental correlation $G(t_1, t_2) = \langle [u(t_1) - u(t_2)]^2 \rangle$ depends only on the time difference $|t_1 - t_2|$ in a power-law fashion for large arguments, $G(t_1, t_2) \sim |t_1 - t_2|^{2H}$, with $0 < H < 1$ called the Hurst exponent of the fBm [54]. In our case, clearly $H = \beta$ [50]. In special cases where the processes preserve ($x \rightarrow -x$) symmetry, which is true for the two limiting cases (AD and SED) discussed in step-fluctuations, a simple scaling argument was given in Ref. [44] to show that $\theta = 1 - \beta$.

The precise definition of $P(t)$ is absolutely crucial for the power-law behavior observed in different papers studying surface fluctuations. Instead of considering the probability of not returning to the initial position, the survival probability, $S(t)$, is defined as the probability of a point on a step not returning in time t to the average step position. As experimental and theoretical studies of different systems have shown, in sharp contrast to the power law decay of the persistence probability, survival probability decays exponentially in time, at long time [47, 48, 49].

$$S(t) \propto \exp(-t/\tau_s), \quad (4.32)$$

where τ_s is the survival time scale.

The exponential decaying property of the survival probability is expected if one applies the theorem [55] which states that if the autocorrelation function $C(t)$ of a stationary Gaussian process decays exponentially for large t , the survival probability must also fall off exponentially, with the survival time τ_s proportional to the correlation time τ_c . The proportionality constant, $c = \tau_s/\tau_c$, which is less than one and independent of the system size L_y , is usually nontrivial [48].

The numerical studies of the first passage probabilities were done for a finite system size. Therefore, the question of how these probabilities are affected by the finite system size is an important one. In the numerical studies of persistence, the persistence exponent was found to increase slightly with the system size. That was found to depend on how large or small the time t is compared to the correlation time which scales as $\tau \sim L_y^z$, and naturally persistence probability is shown to be a function of scaling variable t/L_y^z .

The other parameter these first passage probabilities depend on is the sampling time δt . Already when there was a work pointing to the fact that discrete-time sampling of a continuous-time stochastic process affects the measured persistence probability [56]. This effect is studied in detail for survival probability, $S(t)$. The theoretical and experimental results show that survival probability depends on the sampling time δt [48]. The only time scale in this kind of system is the correlation time τ_c . If there is any scaling involving the sampling time, it should be via the combination $\delta t/\tau_c$. Since the correlation time is proportional to L_y^z , the full function $S(t, L_y, \delta t)$ has the scaling form given in equation (4.33)[48]. The same scaling function was found for both persistence and survival probabilities.

$$S(t, L_y, \delta t) = f(t/L_y^z, \delta t/L_y^z) \quad (4.33)$$

Finally persistence contains information about the universality class of the stochastic process through the exponent θ and its relation to the growth exponent β . Survival probability, on the other hand, provides useful information about the characteristic time scale of the physical mechanism responsible for the underlying step fluctuation in the long-time limit through the survival time τ_s .

4.4 Step-Step Interaction included

We have seen in the first two chapters that step-step interactions are closely related to the distribution of steps on a vicinal surface at equilibrium. However, the theoretical descriptions discussed in the previous section do not take step-step interactions into account. The fact that experimental results are in very good agreement with the theoretical calculations could be due to the weakness of step-step interactions or to the fact that the step under consideration is an almost-isolated step (i.e. far from the next step on the surface). There are theoretical works which explain the way in which different properties are affected by step-step interaction[42, 48]. In the first place the general form of the Langevin equation will be written as [42]

$$\frac{\partial x(y, t)}{\partial t} = -\frac{\Gamma_a}{k_B T} \frac{\delta H}{\delta x} + \eta(y, t) \quad (4.34)$$

where the Hamiltonian H includes the step-step interaction approximated by a confining harmonic potential, $\lambda/2 \int x^2(y) dy$, with λ representing interaction strength.

This interaction term introduces additional term into the Langevin equation [48]. This is equivalent to the Gruber-Mullins mean field approximation discussed in chapter one.

The correlation function for the same step site at different times, $G(t) = \langle (x(t+t_0) - x(t_0))^2 \rangle$, follows a power law [42] with the same exponent as before i.e. 2β where β is the growth exponent:

$$G(t) \sim t^{2\beta}. \quad (4.35)$$

The autocorrelation function $C(t) = \langle (x(t+t_0) - \bar{x})(x(t_0) - \bar{x}) \rangle$, is given by [48]

$$C(t) = 2k_B T \int_{k_{min}}^{\infty} \frac{dk}{2\pi} \frac{\exp[-\Gamma(\tilde{\beta}k^z + \lambda k^{z-2})|t|/k_B T]}{\tilde{\beta}k^2 + \lambda} \quad (4.36)$$

For long time, $C(t)$ remains an exponentially decaying function of time with the correlation time τ_c depending on the interaction strength λ and the step length L_y [48].

$$C(t) \sim \exp(-t/\tau_c) \quad (4.37)$$

Once the autocorrelation is known to decay exponentially in time, we can invoke the theorem [48] used in the previous section and conclude that the survival probability must also fall off exponentially $S(t) \propto \exp(-t/\tau_s)$, with the survival time τ_s proportional to the correlation time τ_c . In the next chapter, results are discussed based on Monte Carlo simulations suggesting the proportionality constant $c = \tau_s/\tau_c$

is still less than one and decreases with increasing the step-step interaction strength.

Chapter 5

Monte Carlo Simulation - Step Fluctuation

5.1 Motivation

There are several experimental and theoretical works which explain the properties reviewed in the previous chapter. The Langevin formalism and all the scaling properties following it are appropriate for an isolated step or at best for such a step with a confining harmonic potential. Some of the agreements we see between the experiments and the theoretical results are perhaps surprising given the fact that in experiments there is an inverse-separation squared interaction between steps that might affect some of the results. The confining harmonic potential is assumed to approximate the inverse-separation squared potential at least when the interaction is not weak and not very strong either. The goal here is to determine whether the properties known for isolated step are affected by step-step interaction and, if they change, how are they modified. In this chapter results from Monte Carlo simulation are presented. In the first part of the chapter we will present simulation of an isolated step to confirm the scaling properties of different quantities discussed in the previous chapter. Next we will discuss how and which of the properties are affected by the step-step interaction. In relation to this we will also present the limitation of approximating the step-step interaction by a confining-harmonic potential. We will further present results showing how the relation between the correlation time

τ_c and the survival time τ_s is affected by the strength of the interaction. Finally the functional form of survival probability will also be discussed.

5.2 Isolated Step

An isolated step is represented by a one dimensional array where the array elements are positions of the step. This representation can be seen as a TSK model or a one dimensional SOS model where the energy is given by

$$E = \epsilon \sum_{i=0}^{L_y-1} |x(i+1) - x(i)| \quad (5.1)$$

A typical configuration of a step is shown below in figure(5.1). The parameters needed to characterize such a step are its length L_y and the kink formation energy

ϵ .

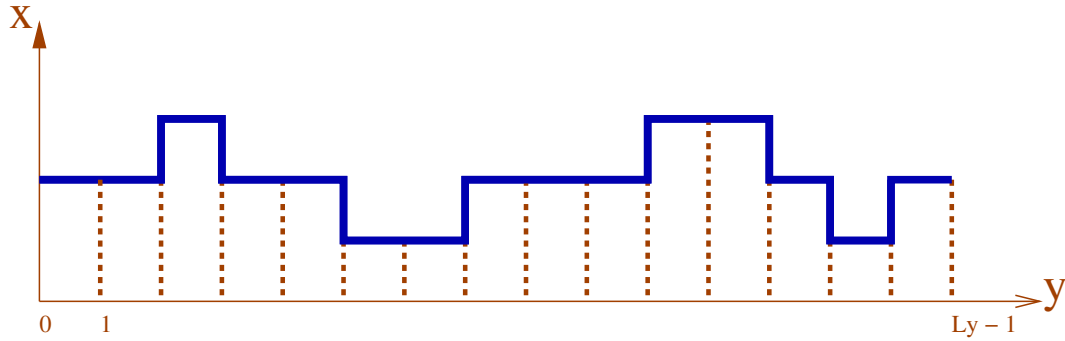


Figure 5.1: Typical TSK representation of an isolated step.

In the simulation, periodic boundary condition is used and the temperature is also specified by setting $kT/\epsilon = 0.5$. The usual Metropolis algorithm is used and the procedure followed is

1. A point on the step is randomly selected.

2. Either +x or -x direction is randomly chosen.
3. The change in energy ΔE is calculated as if the step were to move in the chosen direction.
4. A random number $r(0 \leq r \leq 1)$ is selected and if $r < e^{-\Delta E/kT}$ then the move is accepted otherwise go back to procedure (1).

Repeating the above steps L_y , times so that on average each point on the step has a chance to move, the quantity of interest is calculated.

5.2.1 Width

The width W of the fluctuations defined in Eq. 5.2 is calculated:

$$W = \sqrt{\frac{1}{L_y} \sum_{i=0}^{L_y-1} (x(i) - \bar{x})^2}. \quad (5.2)$$

The initial configuration is a straight step at time $t = 0$. A typical plot of the the width as a function of time for two different step lengths L_y is shown in figure(5.2). As expected the width starts from zero and saturates, at long times, for two different values of the two step lengths. The procedure followed in the Monte Carlo simulation mimics an attachment-detachment(AD) process. In the previous chapter we have seen that AD process belongs to the Edward-Wilkinson (EW) universality class. In accordance with that, we expect the saturation value W_{sat} should scale with the step length as $W_{sat} \sim L_y^\alpha$. The fit to a log-log plot of the W_{sat} vs L_y shown in figure(5.3) gives the roughness exponent to be $\alpha = 0.51$, in agreement with the scaling properties discussed in several works (for example ref.[38]).

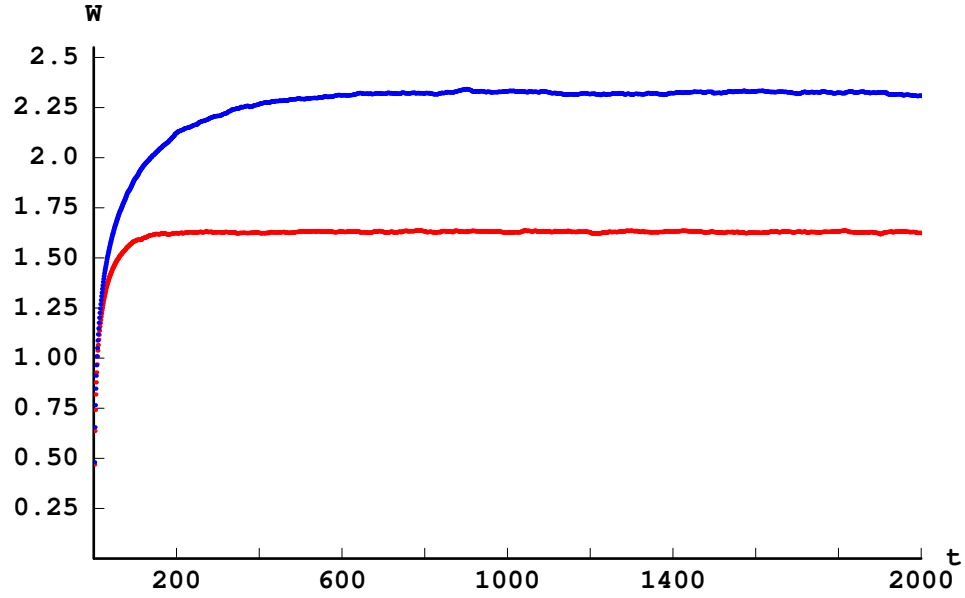


Figure 5.2: Typical plot of width as a function Monte Carlo time for two step lengths: the lower: $L_y = 100$, upper: $L_y = 200$.

5.2.2 Correlations

There are two correlations that have been discussed. Using the well-known properties of their variation with time and the scaling exponents they provide, both of them are used to determine if the Monte Carlo simulation behaves in accordance with the physics we expect to simulate. Later when we discuss the effect of step-step interaction, one of them will be used with the survival probability to see how step-step interaction changes these known properties.

In order to calculate the correlations we needed to find the deviation of each point from the average position. The position of the i^{th} point on the step with respect to the average step position at time t is denoted as

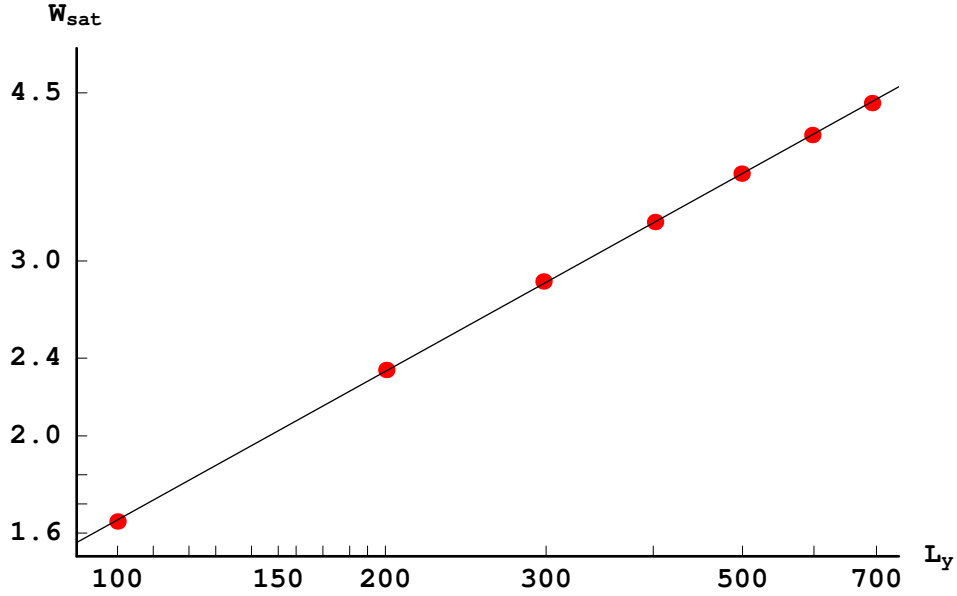


Figure 5.3: The log-log plot of saturation value of the width W_{sat} as a function of step length L_y . The points are found from the simulation. The straight line fit gives a slope of 0.51.

$$dx(i, t) \equiv x(i, t) - \bar{x}(t). \quad (5.3)$$

- **G - Correlation**

This correlation function, usually referred as the time correlation function, is defined as $G(t) = \langle (dx(i, t + t_0) - dx(i, t_0))^2 \rangle$. The averaging is done over different initial times t_0 and over all points i on the step. Typical log-log plot of the G-correlation versus time is given on the figure 5.4. For large time t , it is found to follow a power law $G(t) \sim t^{2\beta}$ with a power $1/2$. This tells us that the growth exponent $\beta = 1/4$. Since we already measured the roughness exponent $\alpha = 1/2$, it indicates we are simulating a system with dynamical

exponent $z = \alpha/\beta = 2$.

As discussed before, the dynamical exponent tells us what kind of limiting process is responsible for the simulated step fluctuation. The measurements of the exponents $\alpha = 1/2$, $\beta = 1/4$, and $z = 2$ are evidence that the dominant process is the attachment-detachment.

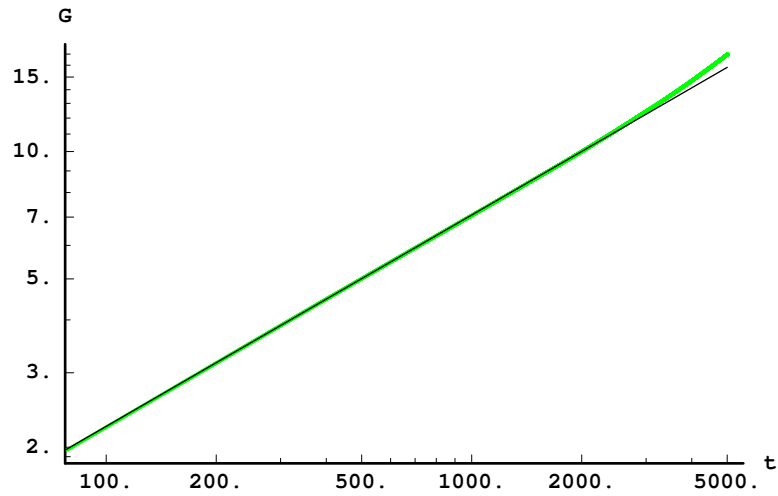


Figure 5.4: The log-log plot of time correlation function (G) as a function of time in MCS with a straight line fit of slope = 0.499.

- **C - Correlation**

The autocorrelation function C is defined as

$$C(t) = \langle dx(i, t + t_0)dx(i, t_0) \rangle \quad (5.4)$$

where the averaging is done over the time t_0 and over all the points i on the step.

Theoretical and experimental works discussed in the previous chapter have

shown that the autocorrelation function decays exponentially with time when the time is much larger than the correlation time i.e. $C(t) \sim \exp -t/\tau_c$ for $t \gg \tau_c$ [41].

A typical log-linear plot of the autocorrelation function as a function of time is shown in the figure(5.5). The large time region of the plot is fitted, and the correlation time is calculated. This was done for several step-lengths, and the log-log plot of the measured correlation time versus the length of the step shows that, indeed, the correlation time has a power law dependence on step-length $\tau_c \sim L_y^z$. The exponent measured from the fit is $z = 2$, which confirms that the process simulated attachment-detachment in agreement with the conclusion arrived by looking at the G-correlation measurement.

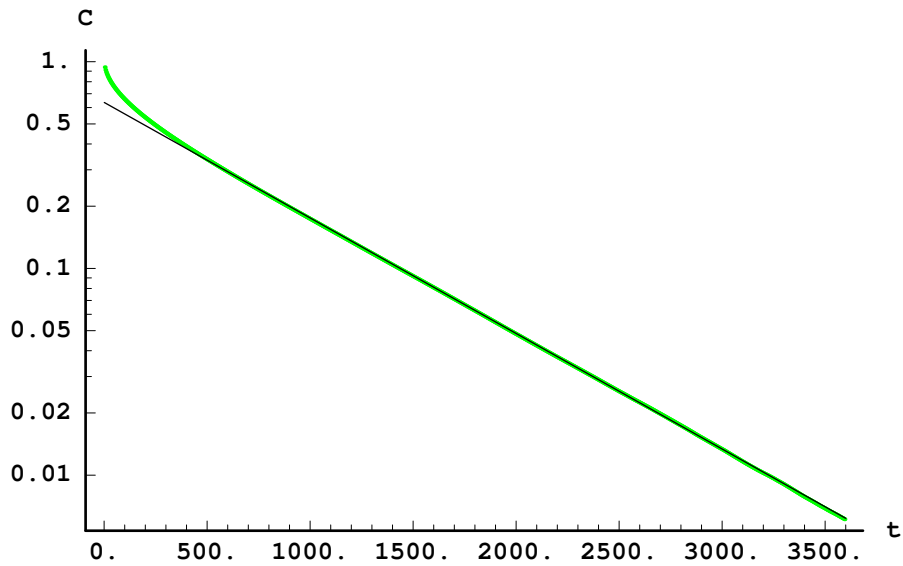


Figure 5.5: The semi-log plot of autocorrelation function ($C(t)$) as a function of time in MCS for a step length of $L_y = 100$ with the fitting line for the long time part.

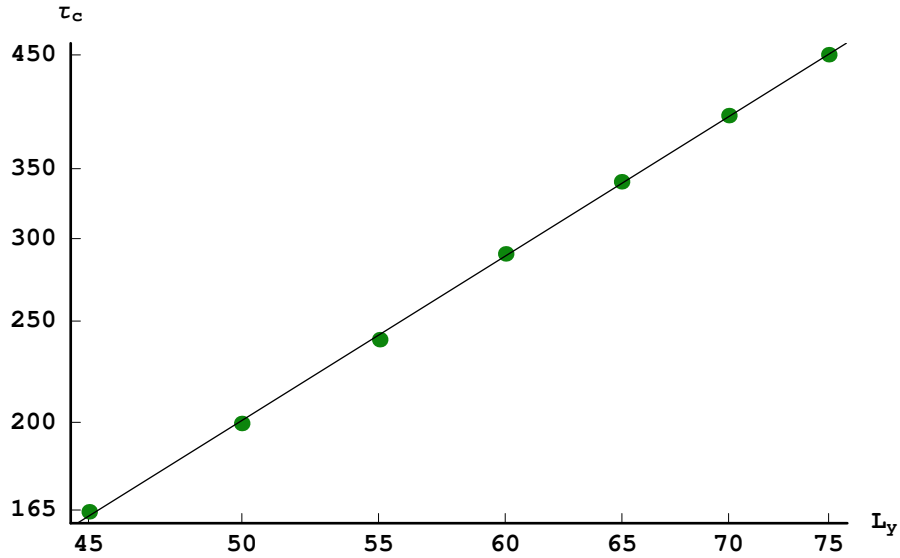


Figure 5.6: The log-log plot of correlation time (τ_c) as a function of L_y . The points are found from the simulation. The line is the fit to the points giving slope = 1.99.

5.2.3 Persistence and survival probability

Persistence $P(t)$ is defined as the probability that a point on the step does not come back to its original position in a time t . As is discussed in the previous chapter, persistence follows a power law with an exponent related to the growth exponent or dynamical exponent,

$$P(t) \sim t^{-\theta}, \quad (5.5)$$

where $\theta = 1 - \beta$ and β is the growth exponent. The log-log plot shown in the figure below indicates that the simulation is fit to a straight line with a slope $\theta = 0.76$. This is in perfect agreement with the theoretical and experimental results discussed earlier.

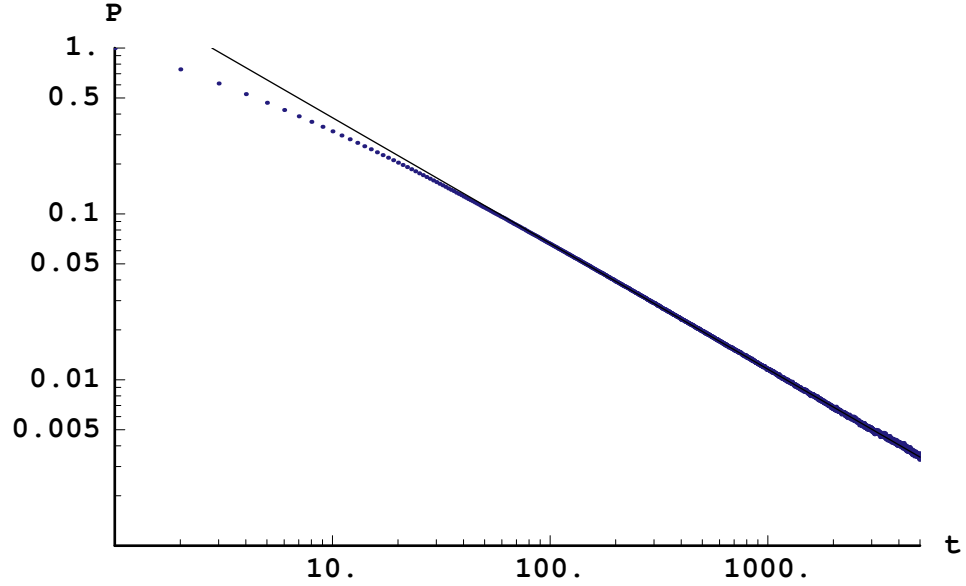


Figure 5.7: The log-log plot of persistence as a function of time in MCS with a straight line fit of the long time part. The slope measured is $\theta = 0.76$.

The other quantity of interest, which resembles persistence by definition but quite different in its mathematical form, is the survival probability. Survival probability is defined as the probability of a point on a step not crossing the average position of the step in a time interval t . By applying the theorem [55] stated in the previous chapter, since the autocorrelation function decays exponentially we expect the survival probability to decay in the same way but with a different time constant.

$$S(t) \sim e^{-t/\tau_s} \quad (5.6)$$

The typical log-linear plot of the survival probability shows that it is exponentially decaying function of time. The time constant τ_s is found to be proportional to the correlation time with ratio $c = \tau_s/\tau_c = 0.5$. This is what one expects from

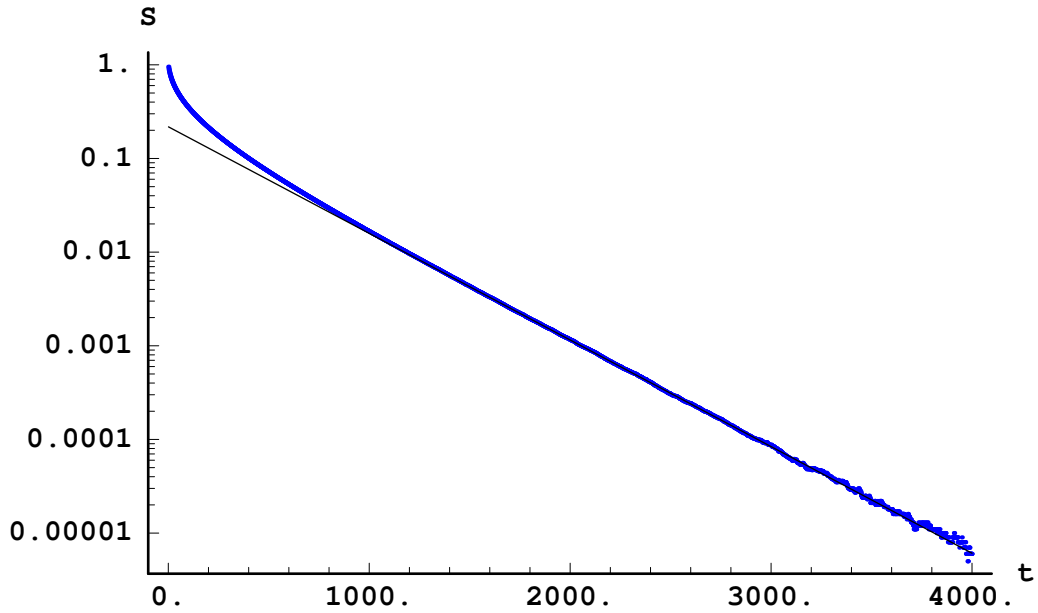


Figure 5.8: The semi-log plot of survival as a function of time in MCS with the linear fit to the long time part.

the theoretical studies cited in the previous chapter.

In the previous chapter we have mentioned that the survival probability weakly depends on the sampling time while the autocorrelation function $C(t)$ does not. In the simulation this assertion is verified by calculating both of these quantities for two different sampling times. The figure below shows that the graphs of the measured autocorrelation function using two sampling times $\delta t = 4$ and $\delta t = 5$ overlap. On the other hand, the measured survival probability for a step length of $L_y = 50$ with sampling times $\delta t = 4$ and $\delta t = 5$ are clearly different.

As is argued in the previous chapter, since the only time scale in this problem is the correlation time, the full functional form of the survival probability should include the ratio $\delta t/L_y^z$.

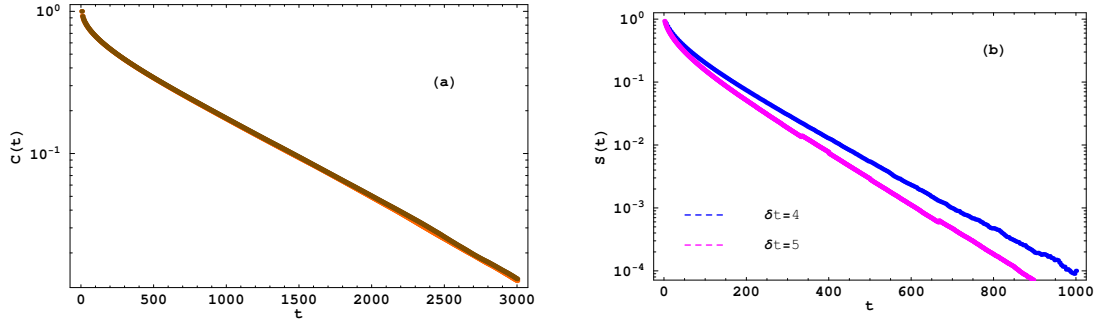


Figure 5.9: (a) The semi-log plot of autocorrelation as a function of time for step length $L_y = 100$ with two different sampling time $\delta t = 4$ and 5. (b) Semi-log plot of the survival probability versus time for step length $L_y = 50$ with different sampling times $\delta t = 4$ and 5.

$$S(t, \delta t, L_y) = f(t/L_y^z, \delta t/L_y^z) \quad (5.7)$$

We can confirm the functional form by measuring the survival probability for different step-lengths L_y , keeping the ratio $\delta t/L_y^z$ constant. This means the graphs of the survival probabilities versus t/L_y^z should collapse onto each other. The figure below shows that indeed the graphs collapse for $L_y = 50, 100, 150$ using sampling times $\delta t = 1, 4, 9$. Although the dynamical exponent was found to be $z = 2$, here it has to be modified to $z = 1.92$ to give the best collapse.

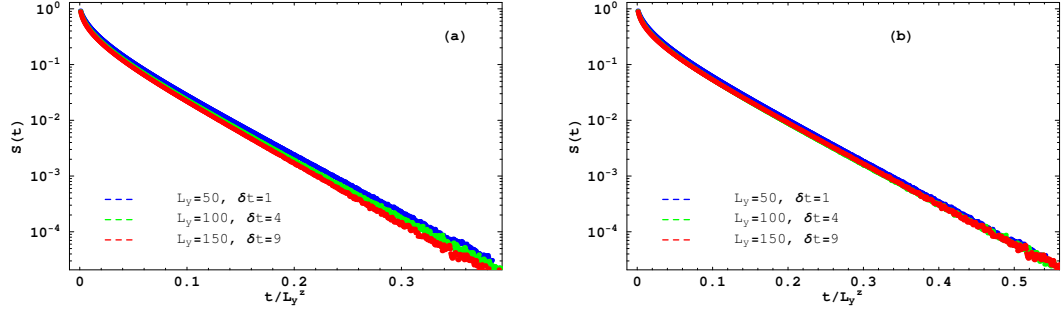


Figure 5.10: The semi-log plot of survival probabilities for three different lengths $L_y = 50, 100, 150$ with three different sampling times $\delta t = 1, 4, 9$, respectively, keeping the ratio $\delta t/L_y^z$ constant. (a) showing poor collapse for $z = 2.0$, (b) the best collapse for $z = 1.92$

5.3 Interacting Steps

The model used in this simulation is the Terrace-Step-Kink (TSK) model, where a surface is represented by the position and number of interacting steps. The number of steps used is 4, with average step-spacing chosen to be 10 and 6 in different considerations. The lengths of the steps are set to 100 except when scaling laws are examined, in which case different lengths are selected. These 4 steps interact with each other via an inverse-separation squared potential. We will see the effect of step-step interaction on different quantities discussed for an isolated step case. First, we will determine if the width scales in the same way as before. Next we will see how the time correlation function and persistence will be affected. We will also present an observed difference in the relation between correlation time τ_c and characteristic survival time τ_s . Finally, the dependence of the survival probability on sampling

time is discussed.

5.3.1 Width

The width is defined as in the previous section: it is the width of the fluctuations of each step, and it is averaged over all 4 steps also. The result is used to determine the time at which the system reaches equilibrium. The initial configuration of the steps is all straight separated by equal distance. The figure below shows that the fluctuation width measured for three interaction strengths, $A = 0.0$, $A = 2.0$ and $A = 10.0$. In all cases it starts from zero and at long time it saturates to a value which depends on the interaction strength as well as the length of the steps. The stronger the interaction is the lesser value of saturation. In the Gruber-Mullins approximation, this is expected to follow the relation $W \propto A^{-1/4}$. We do not see any simple rule relating the saturation value with the interaction strength. However we are interested to see how it scales with the length of steps. That would tell us if the roughness exponent α is the same or it would tell us if this exponent can be defined for a system of interacting steps. As it can be seen in the figure 5.12, the log-log plot of saturation value against step-length is very close to straight line with different exponent for different interaction strength. The exponents measured α are 0.43 for $A = 0.0$ and 0.31 for $A = 2.0$.

5.3.2 Time correlation and persistence

The other quantities we used in the isolated step case to make sure the Monte Carlo is mimicking the attachment-detachment limiting process are the time corre-

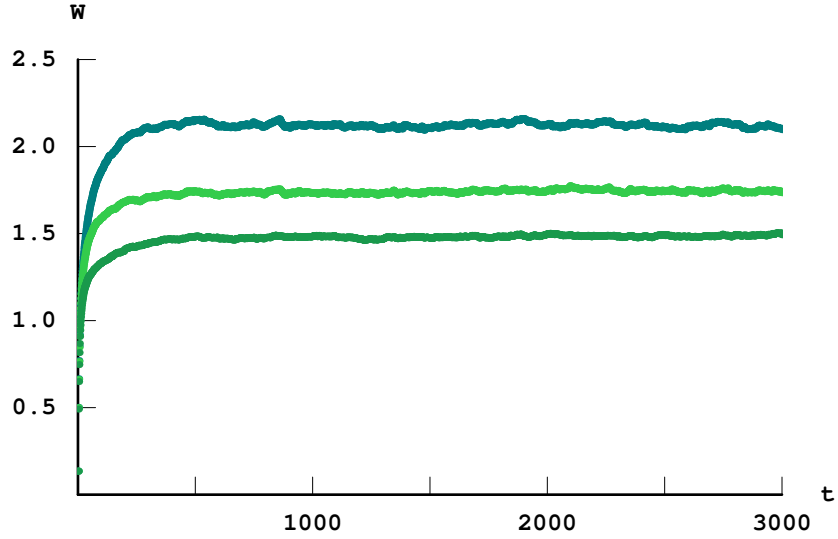


Figure 5.11: The plot of the width as a function of time for a system of 4 steps, length $L_y = 200$, average inter-step distance $L = 10$ and three different interaction strengths. The upper curve is for interaction strength $A = 0$, the middle curve is for $A = 2$, the lowest curve is for $A = 10$.

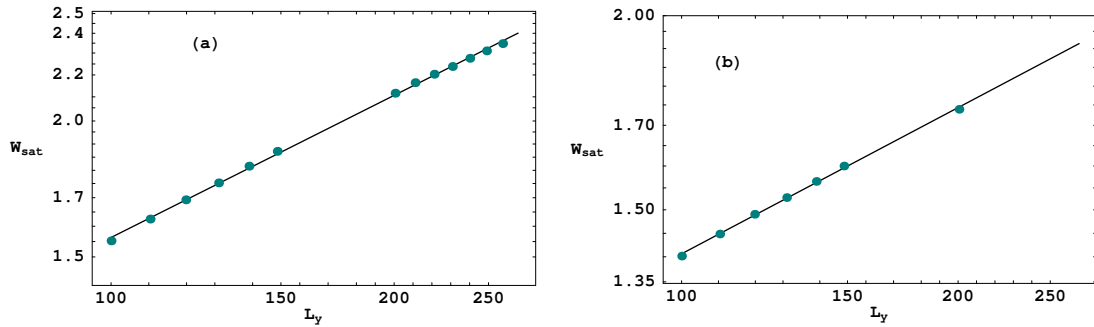


Figure 5.12: The log-log plot of the saturation width versus length of step for 4 interacting steps. (a) Interaction strength $A = 0$ and the fitting line has a slope 0.43, (b) $A=2.0$ and the straight line fit gives a slope of $\alpha = 0.31$

lation (G-correlation) function and persistence. The effect of step-step interaction on time-correlation is discussed in Ref.[42] in a region where a confining harmonic potential is assumed for the interaction. It is shown clearly that the G-correlation scales with time following a power law like in the isolated step case, $G(t) \sim t^{2\beta}$. Here we are considering an inverse-separation squared potential and the property of G is shown to depend on the strength of the interaction.

Step-step interaction is not supposed to change the rate-limiting process at least when a confining interaction potential is considered [48]. In our Monte Carlo studies, the inverse separation-squared potential is being used and for that we want to check that the scaling laws discussed are still valid. As shown in the two figures below, the time correlation follows a power law, $G(t) \sim t^{2\beta}$, with $\beta = 0.250$ for $A = 0$ case and $\beta = 0.244$ when the interaction strength is chosen to be $A = 2$. Clearly, this result depends on the interaction strength.¹

The persistence probability for interaction strength $A=0$ at long time also has a power law, $P(t) \sim t^{-\theta}$, where $\theta = 1 - \beta$. As discussed in the previous chapter, this is true for any stochastic process with zero mean. For the case of $A = 2$, the persistence exponent θ is 0.82 and this not related to the growth exponent measured (i.e. $\beta = 0.24$).

¹Calculating the time correlation needs recording the position of all steps and finding the correlation for each step and average over the number of steps. Rather than finding the correlation for each step separately and averaging over the number of steps. The programs would speed up by 75 % if the summation is done for all steps and average over all points on all steps all together.

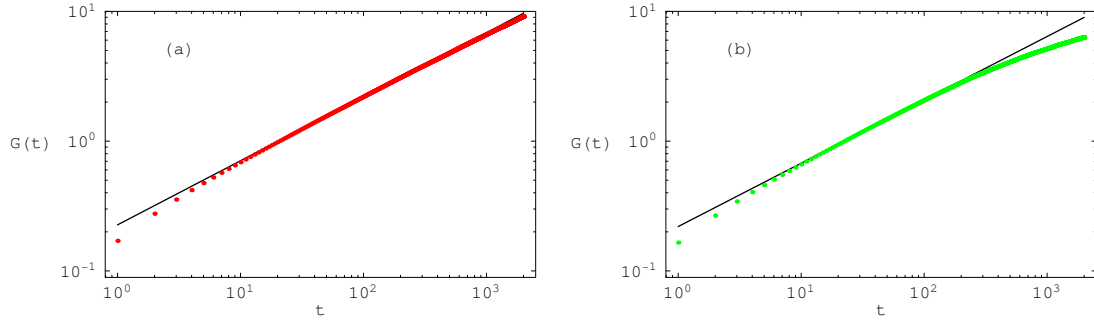


Figure 5.13: A typical log-log plot of time correlation as a function of time in MCS for 4 interacting steps with interaction strength:(a) $A = 0$, the slope of the fit line is 0.500, (b) $A = 2$, the measured slope by fitting is 0.488.

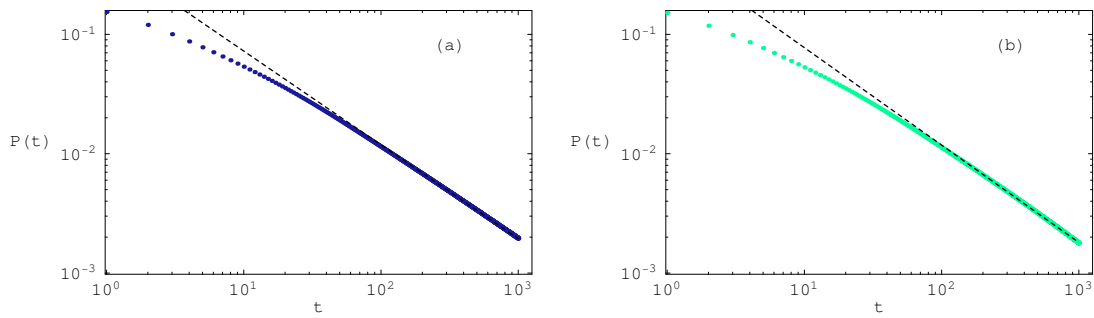


Figure 5.14: A typical log-log plot of persistence as a function of time in MCS for 4 interacting steps with interaction strength: (a) $A = 0$ and the slope of the fit is 0.77 and (b) $A = 2$ where it is fitted to a line of slope 0.82

5.3.3 Autocorrelation and survival probability

The autocorrelation and survival probability are the main focuses of the second half of this thesis. The autocorrelation, or C-correlation as defined in the previous chapter, for an isolated step is known to decay exponentially at long time. We have seen that the correlation time τ_c is the only time scale, and it depends only on the

step length. This has been extended even to an interacting step with a confining harmonic potential, and the autocorrelation is still an exponentially decaying function of time. Now the difference is the correlation time depends on the interaction strength as well as on the step length[48]. Here we have used the more realistic $1/l^2$ -type potential.

The figure below shows that the autocorrelation function is still an exponentially decaying function for long time, with the correlation time depending on both the step length and the interaction strength. Qualitatively, the graphs indicate that the correlation time increases with increasing the interaction strength A . This is in contradiction to what one expects from the result in Ref.([48]):

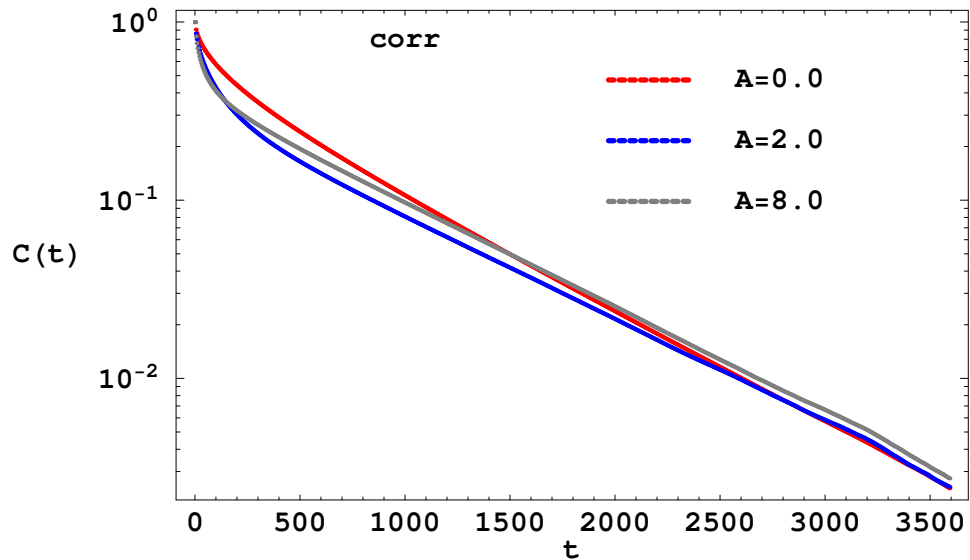


Figure 5.15: Semilog plot of autocorrelation as a function of time in MCS for 4 interacting steps with interaction strength $A = 0, 2,$ and 8 .

In the case of a confining harmonic potential equation 4.36 gives a correlation time

that decreases with increasing interaction strength. The integral equation 4.36 for $C(t)$ is numerically integrated for different λ 's and shown in the figure below confirming that indeed the correlation time τ_c decreases as λ increases.

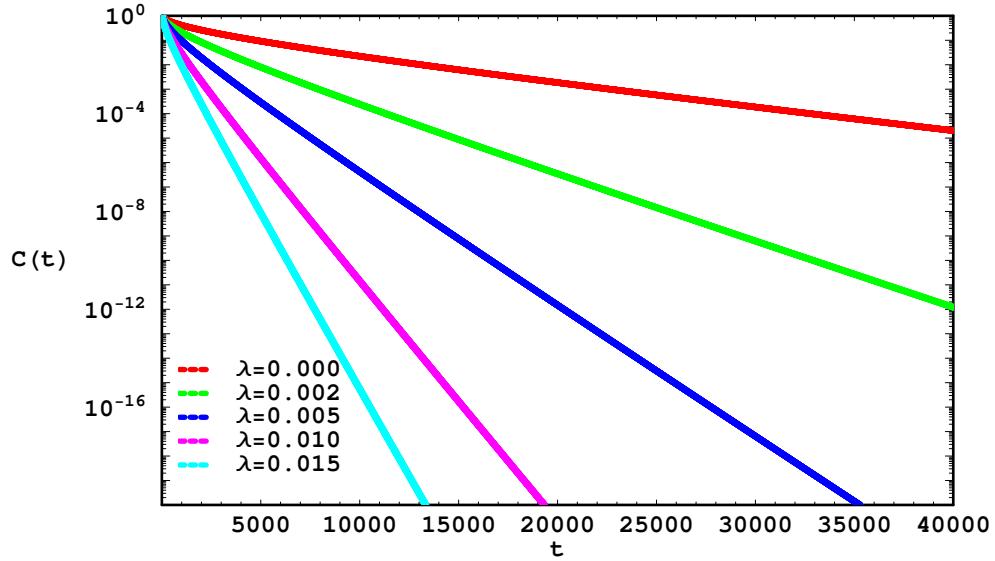


Figure 5.16: Semilog plot of autocorrelation as a function of time obtained by integrating Eq.(4.36) from ref.[48] assuming confining harmonic potential with interaction strength $\lambda = 0, 0.002, 0.005, 0.010,$ and 0.015 .

In order to resolve the contradiction and understand why we have such a difference in the behavior of the correlation time τ_c , two variants of Monte Carlo simulations were performed. In each simulation we considered 4 steps of length 100 and the average spacing between steps to be 6. The first simulation is to check the analytical result reported in reference [48]. Therefore, a simple confining harmonic potential characterized by the strength λ is introduced. As is shown below in fig. (5.17), the correlation time τ_c behaves in the same way as expected from the

analytical result.

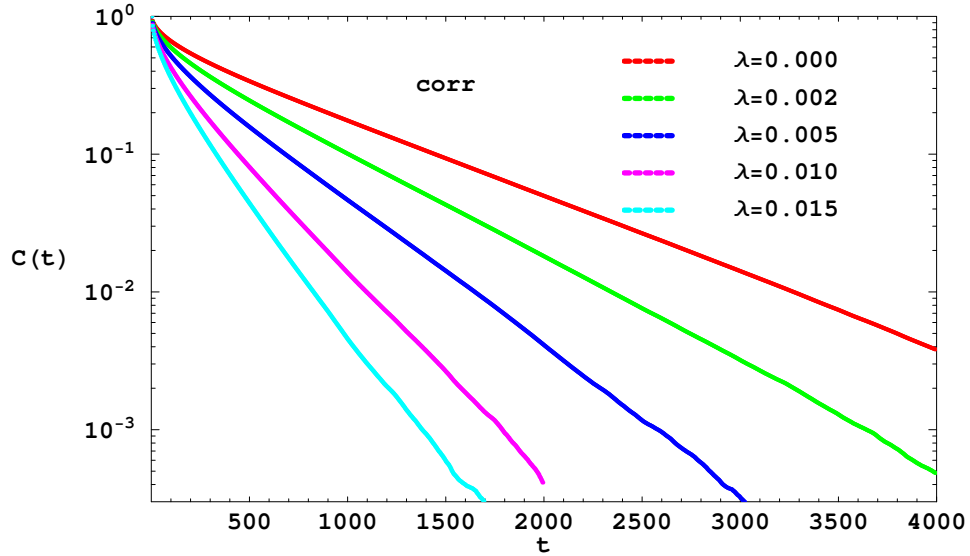


Figure 5.17: Semilog plot of autocorrelation as a function of time obtained from Monte Carlo Simulation using confining harmonic potential with interaction strength $\lambda = 0, 0.002, 0.005, 0.010,$ and 0.015 .

The second Monte Carlo simulation is proposed by noting the difference in the $1/l^2$ and the simple confining harmonic potential case. For the $1/l^2$ -type potential, in-phase meandering of steps does not cost energy whereas in the harmonic potential case, since the expansion is done about a fixed point at a distance L from the neighboring steps, any fluctuation costs energy. Therefore, the harmonic potential case is modified in such a way that it allows for in-phase meandering like in the $1/l^2$ -potential. This is done by approximating the interaction energy by a harmonic-type potential whose minimum-potential point is always moved to the exact middle point from the left and right neighbors. Mathematically, with the necessary boundary

condition in mind, the interaction potential that the j^{th} point on the i^{th} step feels is given by

$$V = \frac{1}{2}\lambda \left[(X[i, j] - X[i - 1, j]) - \frac{X[i + 1, j] - X[i - 1, j]}{2} \right]^2. \quad (5.8)$$

Using this model the autocorrelation function is computed for different interaction-strength λ , and the result indicates that the correlation time increases with increasing λ , which is in agreement with the behavior we found with $1/l^2$ -type potential. This leads us to the conclusion that the Gruber-Mullins description of the interaction potential does not capture all properties of the step fluctuations. In fact, it gives the opposite trend from the correct one.

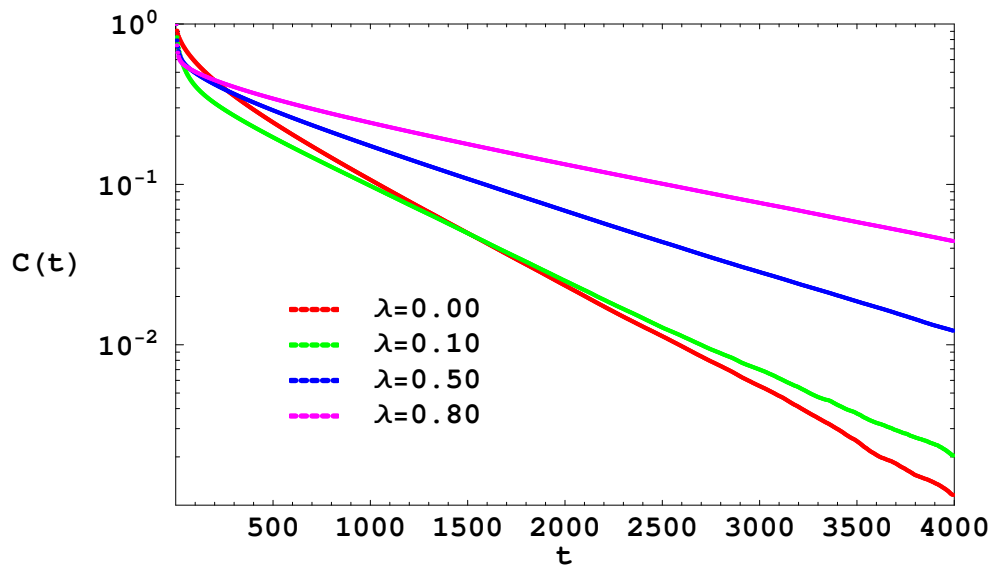


Figure 5.18: Semilog plot of autocorrelation as a function of time obtained from Monte Carlo simulation using moving confining harmonic potential with interaction strength $\lambda = 0, 0.1, 0.5, \text{ and } 0.8$.

In the $1/l^2$ potential, even though the autocorrelation function is different for all different interaction strengths, the time constants τ_c remains the same for $A = 2$ and above. Once we establish the functional form of the autocorrelation to be exponential, we can apply the theorem used before and expect the survival probability to have the same form but different time constant. The theorem suggests that the survival time constant must be proportional to the correlation time with a proportional constant smaller than unity i.e. $c = \tau_s/\tau_c < 1$.

The Semilog plot of the survival probability $S(t)$ versus time t shown in figure 5.19 shows that, indeed $S(t)$ is exponential at long time. The time constants are measured for different interaction strength and the results are shown in the table below. It can be seen that while the correlation time increases, the survival time decreases as the interaction strength A increases. The ratio of correlation time to survival time, $c = \tau_s/\tau_c$ decreases and so remains less than unity as the interaction strength increases.

The full functional form of survival probability is confirmed to be dependent on the time interval in which the step position is measured without any step interaction. Since the only time scale is the correlation time, it was shown to scale with the ratio $\delta t/L_y^z$ because $\tau_c \sim L_y^z$. Does including step-step interaction affect this scaling form? We know the only time scale is still the correlation time; therefore, we expect to have the same scaling form. The figure below shows that for two different interaction strengths, $A = 0.0$ and $A = 0.362$, the graph of survival probability versus t/L_y^z collapses one over the other when it is measured for different step lengths but the same $\delta t/L_y^z$. In order to obtain these collapses the dynamical

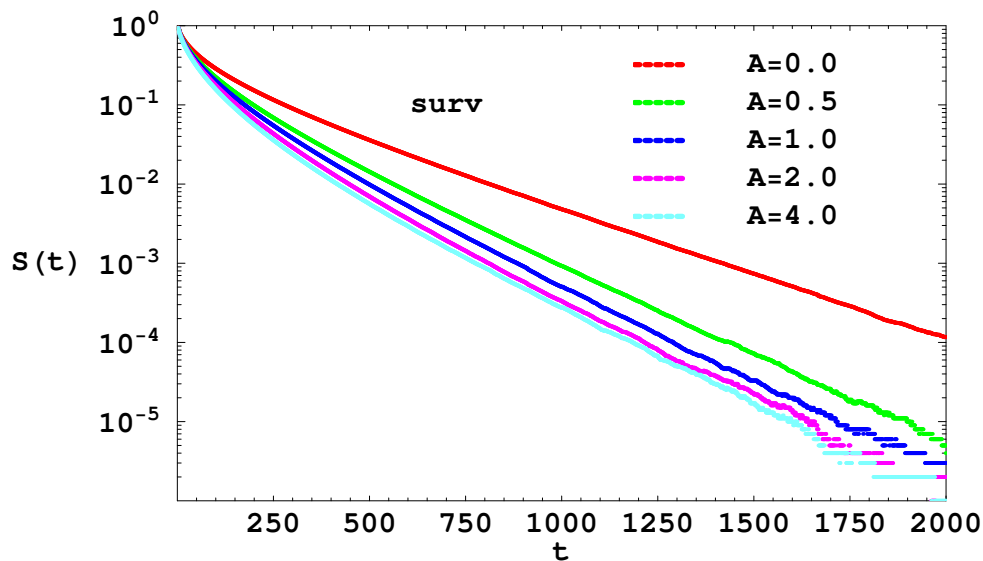


Figure 5.19: Semilog plot of survival probability as a function of time in MCS for 4 interacting steps of length $L_y = 100$ with interaction strength $A = 0, 0.5, 1.0, 1.5, 2.0$.

exponent has to be tuned to different values. The graph for the $A = 0$ case was obtained when $z = 1.8$, while the $A = 0.362$ case is found to have $z = 1.6$.

The scaling form obtained for the isolated step case has to be modified. The correlation time in the system of interacting steps case depends on the interaction strength in addition to the step length. This is already confirmed with the result shown in the above table. Here also, although, the measured dynamical exponent with the step interaction included is $z = 2.0$, to get a good collapse it was tuned to a value quite far from 2. The suggested remedy for this apparent inconsistency is to check the collapse by measuring the survival probability for a number of steps with different length with the same δ/τ_c . In the figure below a semilog plot of the survival

A	τ_c	τ_s	$c = \tau_s/\tau_c$
0.00	692	264	0.38
0.50	730	194	0.27
1.00	752	180	0.24
2.00	762	175	0.23
4.00	762	175	0.23

$\lambda(A)$	τ_c	τ_s	$c = \tau_s/\tau_c$
0.000(0)	775	308	0.40
0.002(0.86)	573	184	0.32
0.005(2.16)	400	104	0.26
0.010(4.32)	297	60	0.20
0.015(6.48)	212	39	0.18

Table 5.1: The measured correlation time, survival time and their ratio as the interaction strength is increased: The upper table for A/l^2 potential for $A = 0.0$ to $A = 4.0$ and the lower one for confining harmonic potential λ varying from $\lambda = 0.000$ to $\lambda = 0.015$.

versus t/τ_c shows that indeed the scaling has to be with the ratio δ/τ_c . Therefore, the full function of the survival probability has to take the following form

$$S(L_y, t, \delta t) = f(t/\tau_c, \delta t/\tau_c). \quad (5.9)$$

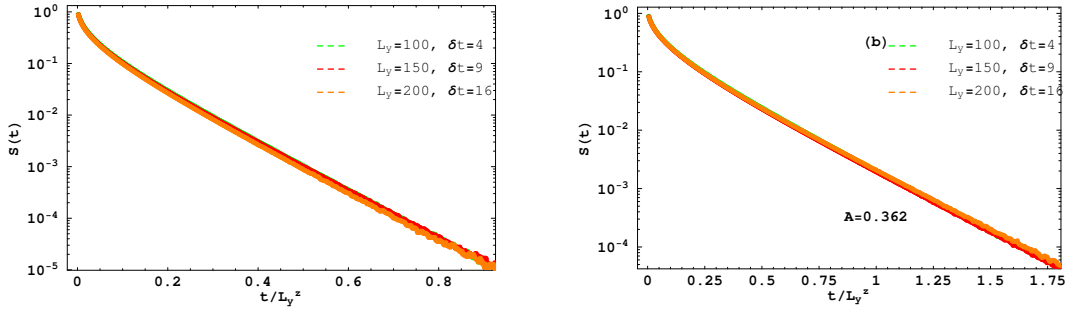


Figure 5.20: The semilog plot of survival probability as a function of t/Ly^z for systems of different three different lengths, $L_y = 100, 150, 200$, but the same $\delta t/Ly^z$. The left and right panels are for $A = 0.000$ and $A = 0.362$, respectively.

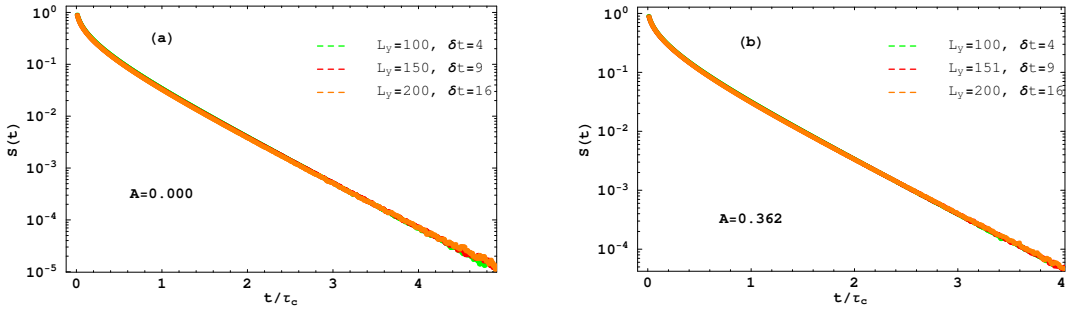


Figure 5.21: The semilog plot of survival probability as a function of t/τ_c for systems of different three different lengths but the same $\delta t/\tau_c$. The left panel is for $L_y = 100, 150, 200$ with $A=0.000$ and the right panel is for $L_y=100, 151, 200$ with $A=0.362$.

Chapter 6

Conclusion

The effect of step-step interaction has been known to be very important in understanding the equilibrium properties of surfaces. The interactions have both entropic and energetic contributions. The entropic repulsion is due to the fact that steps cannot cross. Energetic interaction is due to elastic or electronic dipole-dipole type of interactions. Both interactions are proportional to the inverse of the separation squared. Although they have the same form, when both exist they do not just add together.

Several experiments have been done to determine the strength of the step-step interaction by assuming Gruber-Mullins-type interaction. The Gruber-Mullins approximation is an assumption where a step fluctuates in between two fixed steps. For the case where there is only entropic interaction, the step can be viewed as a path in space-time taken by a one-dimensional free particle in a box, where the time direction is the direction along the step and the spatial direction is the direction perpendicular to the step. The probability distribution of this configuration is a squared sine function with a maximum in the middle of the box and vanishing at the walls of the box. In the case of energetically as well as entropically interacting steps, the potential energy is approximated by a confining harmonic-type interaction potential. In those cases the probability distribution of the terrace-widths are

known to be Gaussian, the same as the probability distribution for a quantum mechanical one-dimensional harmonic oscillator. The distribution is characterized by its variance, which is found to be directly related to the interaction strength.

In the spirit of mapping a single-particle in the box problem to step fluctuation, a system of spinless fermions in one dimension is mapped to a system of interacting steps. Because of the Pauli exclusion principle, the fermions do not cross which is analogous to no-crossing of the steps. The distribution of inter-particle distance is approximated by a generalization of Wigner's surmise coming from random matrix theory. Wigner's distribution is justified for three symmetries (orthogonal, unitary and symplectic) in the ensembles of random matrices. These three symmetries correspond to three particular values of interaction strength. But in physical systems there is nothing special about these three interaction strengths. Therefore, Wigner's distribution is generalized to essentially any value of the interaction strength.

We scrutinized this probability distribution using Monte Carlo simulation using a more realistic inverse-separation squared interaction potential. We have found that the terrace width distribution of a vicinal surface, in particular its variance, is directly related to the step-step interaction strength. The Wigner distribution which approximates the three (orthogonal, unitary and symplectic) ensembles in random matrices seems to describe well the terrace width distribution on a vicinal surface even for values other than the three justified values. The measured values are in good agreement with the expected values from the generalized Wigner distribution. Especially for small values of the dimensionless strength of the elastic interaction \tilde{A} , the Monte Carlo simulation results show that the TWD follows the

generalized Wigner distribution. For larger value of \tilde{A} , the difference between the measured value and what is expected from the generalized Wigner approximation gets larger. In these Monte Carlo calculations only nearest neighbor interactions were used and still the agreement in the small interaction strength region is very good. The disagreement for the large \tilde{A} region can be attributed to the failure of the continuum model.

In our Monte Carlo simulation the system is started from an equally-spaced stepped surface and evolved to its equilibrium configuration. Correspondingly, the variance starts from zero and saturates at a value determined by the generalized Wigner distribution. By using a Fokker-Planck formulation the evolution of the variance of the TWD is analytically calculated and agrees reasonably well with the Monte Carlo result. The analytical result is extended to include experimentally observable initial distributions. For example, one can induce formation of bunched steps and then watch the steps evolve to the equilibrium arrangement. One can also start from equilibrium at one temperature and quench/upquench to another temperature. Both these cases can be described by the Fokker-Planck formulation discussed in chapter 3.

In addition to the step-step interaction strength A , step stiffness $\tilde{\beta}$ and step mobility Γ are the two parameters which characterize a nano size surface. Theoretically, they come in as free parameters in the Langevin formalism for fluctuation of isolated step. This is reviewed in chapter 4. The Langevin equation depends on the rate-limiting process responsible for the fluctuation. The two most common types of Langevin equations describe processes limited by attachment-detachment

and step-edge diffusion. The two processes are characterized by the exponents one finds in the scaling of the width of fluctuations W and the correlation time τ_c with step length.

For attachment-detachment processes the roughness exponent α is $1/2$, the growth exponent β is $1/4$ and the dynamical exponent z is $\alpha/\beta = 2$. For step-edge diffusion limited processes these exponents are $1/2$, $1/8$ and 4 , respectively. Our Monte Carlo simulation is designed to mimic the attachment-detachment process, and this is confirmed in the first results presented in chapter 4. In the system of interacting steps, although the Monte Carlo updating process seems to follow the same dynamics as the isolated step case, the exponents are found to depend on the strength of interaction.

In the isolated step case, the width of fluctuations W increases from zero and saturates to a value W_{sat} dependent on the length of the step. The saturation value W_{sat} follows a power law with an exponent called the roughness exponent $\alpha = 1/2$. In the interacting step case the width increases and saturates at a value dependent not only on the step length but also on the interaction strength. For a fixed interaction strength the saturation value still obeys a power law with an exponent α varying with interaction strength.

The autocorrelation function in the isolated step case is found to follow a power-law decay in a long time regime, $C(t) \sim \exp(-t/\tau_c)$. The correlation time scales with the length of the step in a power law fashion with a dynamic exponent $z = 2$. On the other hand, for the system of interacting steps, although the autocorrelation decays exponentially, the correlation time does not seem to follow a power

law or any other simple rule. However, it is found that as the interaction strength increases, the correlation time increases and approaches a constant limiting value for very strong interaction. This trend of the correlation time is opposite to what was expected from the analytical result found by approximating the step-step interaction with a confining harmonic potential, the conventional mean-field approximation. For the $1/l^2$ -type potential, unlike in the confining-harmonic-potential case, in-phase meandering of the steps does not cost energy. This difference apparently is responsible for the different observed behavior of the correlation time.

The persistence probability is also measured in the simulation of the isolated step and it was found to follow a power law with an exponent $\theta = 0.75$ related to the growth exponent $\beta = 0.25$ which is determined from the measurement of the time-correlation function $G(t) \sim t^{2\beta}$. In the system of interacting steps, both persistence and time-correlation function follow power laws but the exponents do not have the relationship found in the isolated step (i.e. $\theta \neq 1 - \beta$) or any other simple relationship.

Once the autocorrelation function is known to be exponentially decaying function, we can use the theorem to expect the survival probability decaying exponentially with a survival time constant τ_s satisfying the ratio $\tau_s/\tau_c < 1$. This is confirmed both in the isolated and interacting steps simulations. In particular, for the case of interacting steps, the survival time τ_s is found to decrease with increasing interaction strength. The way survival probability depends on time is via the ratio t/L_y^z . It also depends on the sampling time through the ratio $\delta t/L_y^z$. This was confirmed in a simulation of isolated step by keeping the ratio $\delta t/L_y^z$ fixed and

collapsing the graphs of survival probability versus t/L_y^z . In the system of interacting steps, since the correlation time does not scale with step length in a power law fashion, the survival probability functional form is modified to $f(t/\tau_c, \delta t/\tau_c)$. This description seems to fit well when the interaction is not very strong (i.e. $\tilde{A} < 2$). However, for very strong interaction it does not have the same scaling form.

BIBLIOGRAPHY

- [1] C. Herring, Phys. Rev. **82**, 87 (1951).
- [2] M. Giesen, Prog. Surf. Sci. **68**, 1 (2001).
- [3] H.-C. Jeong, E. D. Williams, Surf. Sci. Rep. **34**, 171 (1999).
- [4] T. L. Einstein, O. Pierre-Louis, Surf. Sci. **424**, L299 (1999).
- [5] H. L. Richards, S. D. Cohen, T. L. Einstein, M. Giesen, Surf. Sci. **453**, 59 (2000).
- [6] M. Giesen, T.L. Einstein, Surf. Sci. **449**, 191 (2000).
- [7] A. Videcoq, A. Pimpinelli, M. Vladimirova, Appl. Surf. Sci. **177**, 213 (2001).
- [8] <http://www.fhi-berlin.mpg.de/th/personal/hermann/fccstepskinks.gif>.
- [9] B. S. Swartzentruber, Y.-W. Mo, M. B. Webb, M. G. Lagally, J. Vac. Sci. Technol. A **7**, 2901 (1989).
- [10] B. Joós, T. L. Einstein, N. C. Bartelt, Phys. Rev. B. **43**, 8153 (1991).
- [11] R. Kariotis, B. S. Swartzentruber, M. G. Lagally, J. Appl. Phys. **67**, 2848 (1990).
- [12] X.-S. Wang, J. L. Goldberg, N. C. Bartelt, T. L. Einstein, E. D. Williams, Phys. Rev. Lett. **65**, 2430 (1990).
- [13] E. E. Gruber, W. W. Mullins, J. Phys. Chem. Solids **28**, 875 (1967).

- [14] C. Jayaprakash, C. Rottman, W. F. Saam, Phys. Rev. B **30**, 6549 (1984).
- [15] N. C. Bartelt, T. L. Einstein, E. D. Williams, Surf. Sci. **240**, L591 (1990).
- [16] N. C. Bartelt, T. L. Einstein, E. D. Williams, Surf. Sci. **276**, 308 (1992).
- [17] T. L. Einstein, H. L. Richards, S. D. Cohen, O. Pierre-Louis, Surf. Sci. **493**, 460 (2001).
- [18] M. L. Mehta, Random Matrices, 2nd ed, (Academic, New York 1991).
- [19] F. Haake, Quantum Signatures of Chaos, 2nd and Enlarged ed, (Springer, Berlin 2000).
- [20] T. Guhr, A. Müller-Groeling, H. A. Weidenmüller, Phys. Rep. **299**, 189 (1998).
- [21] F. Calogero, J. Math. Phys. **10**, 2191 (1969).
- [22] B. Sutherland, J. Math. Phys. **12**, 246 (1971).
- [23] W. H. Press, B. P. Flannery, S. A. Teukolsky, W. T. Vetterling, Numerical Recipes, <http://lib-www.lanl.gov/numerical/bookcpdf.html>.
- [24] T. Ihle, C. Misbah, O. Pierre-Louis, Phys. Rev. B **58**, 2289 (1998).
- [25] S. V. Khare, T. L. Einstein, Phys. Rev. B **57**, 4782 (1998).
- [26] N. C. Bartelt, T. L. Einstein, E. D. Williams, Surf. Sci. **312**, 411 (1994).
- [27] B. Blagojević, P. M. Duxbury, Phys. Rev. E **60**, 1279 (1999).
- [28] C. P. Flynn, Phys. Rev. B **66**, 155405 (2002).

- [29] N. C. Bartelt, J. L. Goldberg, T. L. Einstein, et al., Surf Sci. **273**, 252 (1992).
- [30] N. C. Bartelt, J. L. Goldberg, T. L. Einstein, et al., Phys. Rev. B **48**, 15453 (1993).
- [31] H. Gebremariam, S. D. Cohen, H. L. Richards, T. L. Einstein, Phys. Rev. **B69**, 125404 (2004).
- [32] F. J. Dyson, J. Math. Phys. **3**, 1191 (1962).
- [33] D. B. Dougherty, Experimental Studies of Fluctuations and Transport at Solid Surfaces, Ph.D. Thesis, University of Maryland (2004).
- [34] R. K. Pathria, Statistical Mechanics (Butterworth-Heinemann, Oxford, 1999).
- [35] R. Kubo, Rep. Prog. Phys. **29**, 255 (1966).
- [36] M. Ondrejcek, W. Sweich, C. P. Flynn, Surf. Sci. **566-568**, 160 (2004).
- [37] J. Kallunki, J. Krug, Surf. Sci. **523**, L53 (2003).
- [38] A.-L. Barabási, H. E. Stanley, Fractal concepts in surface growth (Cambridge University Press, Cambridge, 1995).
- [39] N. G. Van Kampen, Stochastic processes in physics and chemistry (Elsevier, Amsterdam, 1992).
- [40] R. L. Stratonovich, Topics in the Theory of Random Noise, Vol. I, trans. by R.A. Silverman (Gordon and Breach, New York, 1963).

- [41] O. Bondarchuk, D. B. Dougherty, M. Degawa, E. D. Williams, M. Constantin, C. Dasgupta, S. Das Sarma, *Phys. Rev. E* **71**, 045426 (2005).
- [42] W. W. Pai, N. C. Bartelt, J. E. Reutt-Robey, *Phys. Rev. B* **53**, 23 (1996).
- [43] S. N. Majumdar, *Curr. Sci.* **77**, 370 (1999).
- [44] J. Krug, H. Kallabis, S. N. Majumdar, S. J. Cornell, A.J. Bray, C. Sire, *Phys. Rev. E* **56**, 2702 (1997).
- [45] D. B. Dougherty, I. Lyubinetzky, E. D. Williams, M. Constantin, C. Dasgupta, S. Das Sarma, *Phys. Rev. Lett.* **89**, 136102 (2002).
- [46] D. B. Dougherty, O. Bodarchuk, M. Degawa, E. D. Williams, *Surf. Sci.* **527**, L213 (2003).
- [47] S. N. Majumdar, C. Sire, *Phys. Rev. Lett.* **77**, 1420 (1996).
- [48] C. Dasgupta, M. Constantin, S. Das Sarma, S. N. Majumdar, *Phys. Rev. E* **69**, 022101 (2004).
- [49] M. Constantin, S. Das Sarma, *Phys. Rev. E* **69**, 052601 (2004).
- [50] M. Constantin, C. Dasgupta, P. P. Chatraphorn, S. N. Majumdar, S. Das Sarma, *Phys. Rev. E* **69**, 061608 (2004).
- [51] D. B. Dougherty, C. Tao, O. Bondarchuk, W. G. Cullen, E. D. Williams, M. Constantin, C. Dasgupta, S. Das Sarma, *Phys. Rev. E* **71**, 021602 (2005).

- [52] S. N. Majumdar, C. Sire, A. J. Bray, S.J. Cornell, Phys. Rev. Lett. **77**, 2867 (1996).
- [53] B. Derrida, V. Hakim, R. Zeitak, Phys. Rev. Lett. **77**, 2871 (1996).
- [54] B. B. Mandelbrot, J. W. Van Ness, SIAM Rev. **10**, 422 (1968).
- [55] G. F. Newell, M. Roseblatt, Ann. Math, **33**, 1306 (1962).
- [56] S. N. Majumdar, A. J. Bray, G. C. M. A. Ehrhardt, Phys. Rev. E **64**, 015101 (2001).